1985

# Optical detection of surface vibrations /

Leah M. Akins
*Lehigh University*

# Optical Detection
# of
# Surface Vibrations

by

Leah M. Akins

A Thesis

Presented to the Graduate Committee

of Lehigh University

in Candidacy for the Degree of

Master of Science

in Electrical Engineering

Lehigh University

1985

This thesis is accepted and approved in partial fulfillment of the requirements for the degree of Master of Science.

4/8/1985
(date)

Professor in Charge

Chairman of Department

# Table of Contents

# ABSTRACT

The feasibility of an optical heterodyne technique is studied which is intended for noncontacting measurements of surface vibrations. Previously, holographic techniques have been employed for such purposes, but this technique has the advantage of real time measurements.

Several systems are theoretically investigated leading to the system which was constructed and tested. This system employs envelope heterodyning (optical demodulation) which is an added feature over other approaches. Another feature to be seen is that the distance to the surface under test does not enter into the equations, thus no precise alignments are required. The theory of optical heterodyning and envelope heterodyning is presented. Sensitivity and signal - to - noise ratios are determined theoretically and compared with the experiment.

The limit of sensitivity was around 20 Å of vibrational amplitude.

# 1. INTRODUCTION

This paper is concerned with the feasibility study of an optical probe used to measure small surface vibrations. The system utilizes a Bragg cell to modulate the light at 80 MHz and an electro-optic crystal for demodulation. Information on the surface vibration can be determined from the speckle field which is reflected from a test object with a rough surface or from specular reflection. The experimental part of this study deals only with specular reflection.

The report proceeds in the following order. In section 2, an overview of existing systems is presented. Section 3 investigates the speckle field and the requirement for its coherence. Section 4 contains the complete theory of the optical heterodyne technique to be used in the measurement of surface vibrations. This includes discussions of the modulating processes of the Bragg cell and the electro-optic crystal modulator. Also, the derivation of the frequency components at the output of the system is given which leads to the formula for finding the amplitude of the surface vibration. The complete optical system is described along with the required detection electronics. Section 5 contains the determination of the sensitivity and the signal - to - noise ratio of the experimental system which is then compared with the derived signal - to - noise ratios of similar probes. In section 6, the system constructed is presented and the test procedure is explained. The final section

presents the results and the final conclusions made.

The system constructed was found to be capable of measuring surface vibrations on the order of tens of angstroms. In the report, comparisons are made to sytems employing similar techniques. Though it was found that the sensitivities of the different systems do not vary greatly, the system presented in this paper is assuredly less complex and possible less costly.

# 2. Overview of Existing Systems

Acoustic surface wave amplitude and phase measurements are a concern in the investigation of acoustic systems. A need for these measurements has arisen in certain nondestructive testing applications. Prior to the development of the optical probe, the instruments that were available to make such measurements were a piezoelectric point probe and a probe which is electrostatically coupled to the measurement surface[1]. Both these techniques have complicating disadvantages, such as: (1)require the maintenance of a constant pressure, (2)limited to relatively low frequencies, (3)the electrostatically coupled probe is applicable only when the measurement medium is piezoelectric, and (4)the use of any tangible probe is bound to perturb the acoustic field distribution to some extent which is not readily known.[1] The optical probe does not have these disadvantages, it has a negligible effect on the surface wave.

The basic principle for all optical probes is that a laser beam reflected from a surface is phase-modulated by the test surface displacements. The phase-modulated optical signal must be converted to an amplitude modulated electrical signal which retains the phase information. Since photodetectors are insensitive to optical phase, the conversion to amplitude modulation must take place in the optical system by means of some form of interferometer.[1] A carrier frequency may be introduced to im-

prove system stability and facilitate electronic signal processing. Since there are many forms of interferometers and many different ways to implement a carrier frequency if so desired, many different optical systems have been developed to function as an optical probe. All of these systems can be represented symbolically by Fig 2.1, (from De La Rue, et.al., reference 1).

All the optical probes are based on some form of an interferometer, therefore the laser beam is split into a signal beam 'S' and a reference beam 'R', as shown in Fig. 2.1. Depending on the choice of systems, each of these beams may or may not be phase modulated by a carrier frequency $f_b$. The test sample modulates the signal beam at frequency $f_s$ and this optical signal is directed to the photodetector. The reference beam may also be modulated at $f_s$ for particular optical systems. Finally, the signal and reference beams are recombined on the photodetector surface.

Expressions for the detected amplitudes of the signal and reference beams can be readily obtained using the block diagram in Fig. 2.1. The factors $\alpha_s$ and $\alpha_r$ are introduced to account for the attenuations in S and R as a result of losses in various optical components and modulators. Then, assuming the phase modulation at frequency $\omega_s$ to take the form of a cyclic optical path variation, the detected amplitudes $S_d$ and $R_d$ can be written in the form given by eq. 2.1.*

$$\begin{aligned} S_d &= \alpha_s S \exp i[k\{L_s+\delta_s\cos(\omega_s t+\theta_s)\}-(\omega_0+p\omega_b)t] \\ R_d &= \alpha_r R \exp i[k\{L_r+\delta_r\cos(\omega_s t+\theta_r)\}-(\omega_0+q\omega_b)t] \end{aligned} \qquad (2.1)$$

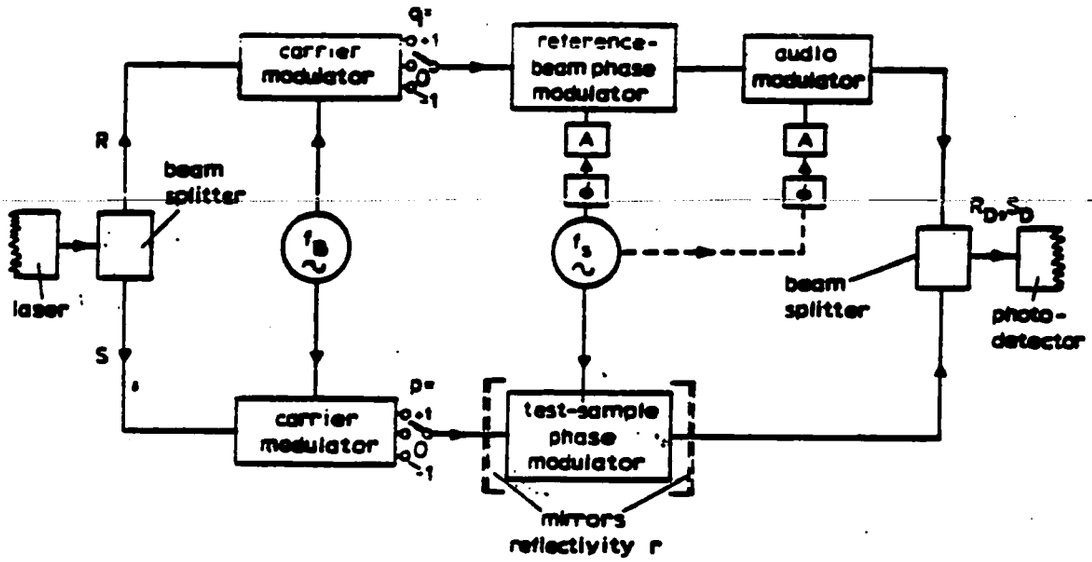


Fig. 2.1 *Block Diagram of General Optical System.*[1]

The variables in eq. 2.1 have the following meanings:

S(and R)=the initial amplitude of the signal (and reference) wave, normalized so that the initial power in the signal (and reference) beam is SS* (and RR*).

$\omega_0$=laser frequency

$\omega_s$=frequency of test object vibration

$\omega_b$=carrier frequency

$L_s$ and $L_r$=signal and reference beam path lengths

$\delta_s$ and $\delta_r$=test object and reference phase modulating amplitudes at frequency $f_s$

$\delta_s$=amplitude of normal target surface vibration
$\delta_r$=optional reference beam phase modulation amplitude (analogous to $\delta_s$)

p and q= -1, 0, +1, depending on the switch position in Fig. 2.1.

p(or q)= -1, downshifting of R(or S) by $f_b$
p(or q)= 0, no frequency shifting of R(or S)
p(or q)= +1, upshifting of R(or S) by $f_b$

k=optical propagation constant

$\alpha_s$ and $\alpha_r$=attenuation factors of signal and reference beams

(*note: same notation used in Reference 1).

The light intensity, $N_d$, is then given by:

$$N_d \propto (S_d+R_d)(S_d^*+R_d^*). \tag{2.2}$$

By replacing eqs, 2.1 into eq. 2.2, multiplying out the terms and using various trigonometric identities, a more interesting form for $N_d$ can be found:

$$N_d \propto (\alpha_s^2 S^2+\alpha_r^2 R^2)+\alpha_s\alpha_r SR\{2\cos\phi-2k\delta_s\{\sin(\phi+\omega_s t+\theta_s)+\sin(\phi-\omega_s t-\theta_s\}$$
$$+2k\delta_r\{\sin(\phi+\omega_s t+\theta_r)+\sin(\phi-\omega_s t-\theta_r)\}\} \tag{2.3}$$

where $\phi=k(L_s-L_r)+(q-p)\omega_b t$. In eq. 2.3 it has been assumed that $k\delta_s \ll 1$ and $k\delta_r \ll 1$ since the amplitudes of vibrations of interest are fractions of the laser wavelength. A complete analysis for the derivation of eq. 2.3 for the experimental system investigated in this report can be found in appendix B.

Note from eq. 2.3 that there are components of the light at several frequencies. Depending upon the values of p and q, one of the frequency components will have an amplitude directly proportional to $\delta_s$. The type of system developed for particular values of p and q can be categorized into two divisions: an optical homodyne system and an optical heterodyne system. For the homodyne technique $(p-q)=0$, which results in a system where the signal and reference beams at the detector are the same frequency but different phase. For the heterodyne technique $(p-q)\neq 0$, which results in a system where $S_d$ and $R_d$ are at different frequencies causing 'mixing' to occur at the detector. This generally means that a carrier frequency was introduced into the system.

An overview of the most common optical probe systems can be found in Table 2.1 (from De La Rue, et.al., Reference 1). Both homodyne and heterodyne techniques are included. The second and fourth columns are concerned with a carrier frequency modulation imposed on the beam and if so, whether the detected frequency is shifted from the acoustic frequency. Shifting of the detected frequency can be an important advantage because it allows discrimination between spurious signals and the

COMPARISON OF PROBE SYSTEMS

| Probe | System (see Fig. 2.1) | Reference | Output signal frequency-shifted | Output signal independent of optical phase? | Comments |
|---|---|---|---|---|---|
| 1 | $(p-q)\omega_b=0$<br>$\delta_r=0$<br>e.g. 'homodyne' | 2 | no | no | Requires optical-path-length control loop for acceptable stability; phase reference by comparison with electronic $\omega_s$ signal; usable at $\omega_s$ down to DC |
| 2 | 'Homodyne'<br>$(p-q)\omega_b=0$<br>$\delta_r\neq 0$ | | no | no | Optoacoustic phase comparison requires a transducer to vibrate reference mirror; reference and signal-vibration amplitudes must be equal; need pathlength control loop; usable at $\omega_s$ down to DC |
| 3 | $(p-q)\omega_b\neq 0$<br>$\delta_r\neq 0$<br>e.g. Bragg cell heterodyne | | yes | yes | Simple receiver. Frequency shift gives chopper effect; electronic filtering problems at low $\omega_s$; reference and signal-vibration amplitudes must be equal |
| 4 | $(p-q)\omega_b\neq 0$<br>$\delta_r=0$<br>local oscillator signal electronically derived | | yes | no | Coherent detection, but not phase-stable; frequency shift gives (radiative) chopper effect; electronic filtering problems at low $\omega_s$ |
| 5 | $(p-q)\omega_b\neq 0$<br>$\delta_r=0$<br>optically derived l.o., e.g. Bragg cell heterodyne | this paper, 1,3 | yes | yes | Phase-stable coherent detection; frequency-shifting chopper effect; filter problems at low $\omega_s$; output signal can be compensated for variations in optical intensity |

COMPARISON OF PROBE SYSTEMS (continued)

| Probe | System (see Fig. 2.1) | Reference | Output signal frequency-shifted | Output signal independent of optical phase? | Comments |
|---|---|---|---|---|---|
| 6 | $(p-q)\omega_b \begin{cases} \neq 0 \\ =0 \end{cases}$ R=0 e.g. Fabry-Perot | | yes no | yes | Optical cavity gives much greater sensitivity; low frequency shift used to give pick-up rejection; automatic-spacing-control loop essential; no reference beam required; usable at low $\omega_s$; broadband spatial-frequency capability |
| 7 | $(p-q)\omega_b = \omega_s$ near-field e.g. knife edge | 3 | no | yes | Poor performance at low $\omega_s$; narrowband spatial-frequency capability; quantitative amplitude measurements diffucult; signal-amplitude is orientation dependent; zero-order and 1st-order beams are reference and signal beams, respectively; alignment of these beams is automatic |
| 8 | $(p-q)\omega_b = \omega_s$ far-field recombination | | no | no | Acoustic surface wave gives frequency-dependent beam-splitting angle; has highest frequency capability |

Table 2.1 *Comparison of probe systems.*[1]

desired optoacoustically generated signal.[1] The second column also indicates whether the reference beam is phase modulated at frequency $\omega_s$ which is used to give an acoustic wave phase reference. The fifth column gives information on whether or not the final signal is dependent on undesired optical phase variations which can be due to vibrations, thermal expansion, etc..

Both homodyne and Fabry-Perot probes (probes 1, 2, and 6) may be used at low frequencies. These probes require an optical path length control loop to maintain stability. In these probes, acoustic phase is most readily measured by comparing the detected signal phase to the signal source phase. The near-field probe (probe 7) is simple and rugged but ther are a number of disadvantages. For one, quantitative amplitude measurements are diffucult because the signal amplitude is dependent upon orientation. Also, the probe is ineffective at relatively low frequencies since this implies inconveniently long focal lengths for the lens' used in the optical set-up. Yet, the upper limit on frequency, $\omega_s$, is determined by the spatial frequency at which the diffraction orders separate out, i.e. for a lens of focal length 0.25 cm and acoustic wave velocity of $3\times10^3$ m/s, the upper frequency limit is 2 GHz.[1] The far field probe (probe 8), where the zero diffraction order and first diffraction order are superimposed at the photodetector in the far field, has the highest frequency capability which is only limited by current available photodetectors. Its principle advantage is in situa-

tions where high frequencies must be measured which would require optical components to be located inconveniently close to the surface in the other probes. In the heterodyne probes (probes 3, 4, and 5), separation of the sideband at frequency $(q-p)\omega_b \pm \omega_s$ from the carrier becomes exceedingly diffucult as $\omega_s$ is lowered. The problem is magnified at low frequencies since the carrier amplitude is much greater than the information-carrying sideband amplitude. The upper frequency limit for these probes is higher than most of the other probes (except probe 8) and is similar to that of the near field probe (probe 7).

The type of probe investigated in this report is probe 5 using an optically derived local oscillator, which was implemented with a Bragg cell. De La Rue, et.al., in Reference 1, chose probe 5 also for their experiments because "it requires the most complex detection electronics, but provides the most versatile and precise information acquisition and display system."[1] For the sake of comparison, optical set-ups for De La Rue's probe[1] and examples of probe types 1, 5, and 7 can be found in appendix A. A variation upon probe 5 was investigated which entailed optical demodulation using an electro-optic crystal. This was included in the system which was constructed and tested, as described in detail further on in the report. Using this variation, it was found that the complexity of the detection electronics was notably reduced.

# 3. Specular Reflection vs. Speckle Field

Optical detection of surface vibrations is based on the assumption that the laser light reflected from the surface is coherent. For the sake of generality, the surface is assumed to be rough. If the surface is smooth, i.e. a mirror, then the reflected light is coherent. This section discusses coherence and specular reflection, the speckle field, which is an interference pattern formed when laser light illuminates a rough surface, and what can be said about the coherence of the speckle field.

## 3.1 Specular Reflection

Laser light exhibits two types of coherence: *spatial* coherence and *temporal* coherence. Spatial coherence characterizes the spatial variation in coherence across the wavefronts in the direction transverse to the propagation direction. A light wave which exhibits spatial coherence infers that knowledge of the electric field at one point on the wave at time t, yields information about the electric field at every point on the wave at the same time t. Temporal coherence refers to the correlation between the wave at one point and the wave at the same point at a later time. Thus, for a light wave which demonstrates temporal coherence, information about the electric field at a point on the wave at time t implies the value of the electric field at that point for all time after t.[4]

Specular reflection refers to reflection from a mirror. When laser light is reflected from a mirror, the coherence of the light is maintained. This is because each point on the wave is reflected in phase from a mirror and, as can be inferred from the above discussion, this does not affect the spatial and temporal coherence of the laser light. The coherence of light is an important concern in this report since a strong degree of coherence is necessary to produce a clear interference pattern. Detections of variations in the interference pattern will lead to the desired information. The coherence of light reflected off a rough surface is not so easily guaranteed, this is explained in the following discussion.

## 3.2 Speckle Field

When laser light is reflected from a rough surface, one usually notices a peculiar tecture to the light - a sparkling or speckled pattern. This pattern is referred to as *laser speckle* and is due to interference. Each point on the surface scatters the light as a spherical wave and thus the surface can be approximated by a collection of a large number of closely packed point sources. Because of the roughness of the surface, the relative phases of these point sources are random though they are constant in time if the surface is not moving. Thus, if the reflected field is viewed on a screen, at any given point there are wave contributions from a number of different points on the illumi-

nated surface, each with a random phase. The superposition of these waves can have a very large or very small net electric field. The result is an interference pattern that is highly irregular - the speckle field (see Fig 3.1).

A discussion of the restrictions for coherence of the speckle field is the next logical step. Consider a light source made up of many narrow, closely-packed point sources (Fig. 3.2). For 2y on the order of $\lambda$ or larger, the waves in directions 1, 2, and 3 are independent of one another and the resulting radiation is incoherent. The light source in Fig. 3.2 can be represented by a series of single radiating plane elements of total width 2y; this is clarified by the hash marks in Fig. 3.3. Every single plane element is able to change its phase. Thus, for the resulting wave in direction 1, only the amplitude changes regardless of which element on 2y is changing phase. This is not the case for the oblique directions, such as 2 or 3. For these directions there is an additional phase difference which depends upon which element is phase changing. The difference in the paths for the directions 1&2 or 1&3 have the same maximum value; $\Delta s_2=\Delta s_3=2y\sin u$, regardless of relation to the upper most or lower most plane element.

Statistically, the path differences have the same average value: $\overline{\Delta s}_2=\overline{\Delta s}_3=\frac{1}{2}(2y\sin u)$. The sum of these two average values is $\overline{\Delta s}=2y\sin u$. This dependent path difference, $\overline{\Delta s}$, from the


Fig. 3.1 *Sketch of a magnified speckle field.*

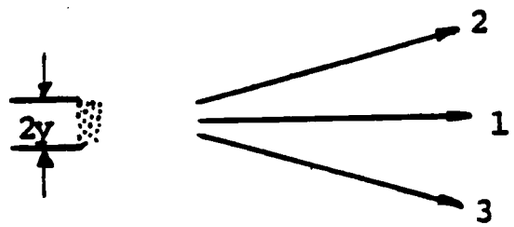


Fig. 3.2 *Light source made up of many equal frequency point sources with random phases.*

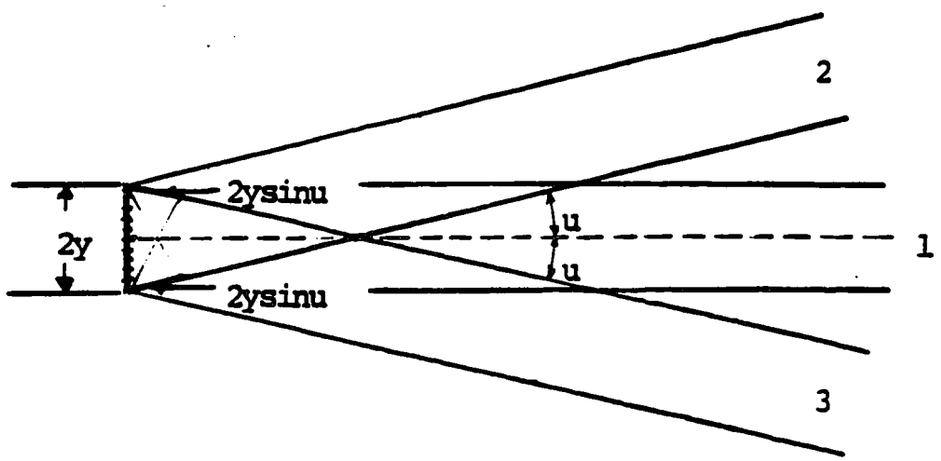


Fig. 3.3 *To derive the coherence relation.*

location of the plane elements can only be neglected if $\overline{\Delta s}=2y\sin u<<\lambda/2$.[5] Thus a light source of diameter 2y as shown in Fig. 3.2 can be replaced by a point source only for the radiation pattern within a bounded angle 2u, where 2y and u must fulfill the following inequality:

$$2y\sin u<<\lambda/2 \quad . \tag{3.1}$$

Eq. 3.1 is defined as the *coherence relation*.[5] If the coherence relation is fulfilled then the radiation is said to be coherent.

In light of the above discussion, the reflection of laser light from a rough surface can be thought of as a light source as shown in Fig. 3.2. It is noted from the coherence relation (eq. 3.1) that the diameter 2y plays a large role in the attempt to get a clear interference pattern. Thus, to ensure coherent speckles, the laser light may be focused onto the surface making 2y very small. Also, the solid angle within which detection will occur should be small. This assures that 2ysinu is much less than $\lambda/2$ thus fulfilling the coherence relation. If this can be accomplished, then the light within a speckle is coherent and such an individual speckle can be projected on the photodetector and brought to interference with the reference beam.

# 4. Optical Heterodyne Detection

In section 2 (Overview of Existing Systems), a block diagram of a general optical heterodyne system was depicted. Several different types of probes were discussed and a probe was chosen for investigation for which a carrier frequency is impressed on the beam. In this section the design of such a particular optical heterodyne detection system will be presented. This will include the description of special optical components, the derivation of the amplitudes of detected frequency components, and the optical set-up. This system also includes a detection scheme of 'envelope heterodyning', which does not seem to have been used before.

## 4.1 Optical Components of Special Interest

Before describing the optical system it is necessary to have an understanding of the special optical components which are used in the system. These are the Bragg cell and a light modulator which uses the linear electro-optic effect in a crystal.

### 4.1.A The Bragg Cell

The Bragg cell is an acousto-optic cell which may be used to divide a light beam into several beams with different frequencies and directions. If a standing acoustic wave is pre-

sent in a medium then a spatially periodic gradient in the refractive index of the medium is created which is proportional to the acoustic wavelength. This is illustrated in Fig. 4.1. Using a geometric analysis of the pathlength difference between abc and a'b'c', an equation for the angle of the reflected beam is found

$$\phi_k = \sin^{-1}(k\lambda/2\lambda_a) \tag{4.1}$$

where $\lambda$=wavelength of laser light in the medium. Note that when the air-cell-air interface is accounted for a similar equation is arrived at

$$\phi_k = \sin^{-1}(k\lambda_0/2\lambda_a) \tag{4.2}$$

where $\lambda_0$ is the wavelength of the light in air and $\phi_k$ is the angle at the output of the Bragg cell. The interfaces are vertical in Fig. 4.1. If the incident angle of the light is such that the pathlength difference is $\lambda$, then eq. 4.2 becomes

$$\phi_k = \sin^{-1}(\lambda_0/2\lambda_a) \quad . \tag{4.3}$$

This is called the Bragg angle.

Now consider that the acoustic waves are travelling through the medium. Thus, each point on the incoming wavefront sees a periodic change in the refractive index where the refractive index is changing at a rate proportional to the velocity of the acoustic waves and consequently the acoustic frequency. This changing index of refraction results in modulation of the output angle. Thus, if an optical detector is placed at a fixed position to receive the acoustic carrier modulated

reflected light, the detector would observe amplitude modulated light proportional to the acoustic frequency. The frequency of the reflected beam for an angle, $\phi_k$, is given by

$$f_k = f_0 \pm kf_a \tag{4.4}$$

where $f_0$ = laser frequency and $f_a$ = acoustic frequency. If the incident beam intersects the acoustic waves at the Bragg angle, $\phi_b$, and more than a full acoustic wavelength is traversed by the light path, then the light intensity tends to be concentrated in the reflected light beam with frequency

$$f_b = f_0 \pm f_a \quad . \tag{4.5}$$

As a final note on the Bragg cell, the intensity of the light in each reflected beam depends on several parameters including the cell dimensions, the acoustic and light frequencies, the acousto-optical material, the electrical power used to drive the transducer, and the angle between the acoustic wavefronts and the incident beam. For this experiment a Bragg cell was obtained for 80 MHz modulation of 632.8 nm laser light (HeNe laser wavelength). The Bragg cell was operated at the Bragg angle and the intensity of the zero-order and first-order beams was controlled by varying the electrical power to drive the transducer, see Fig. 4.2.

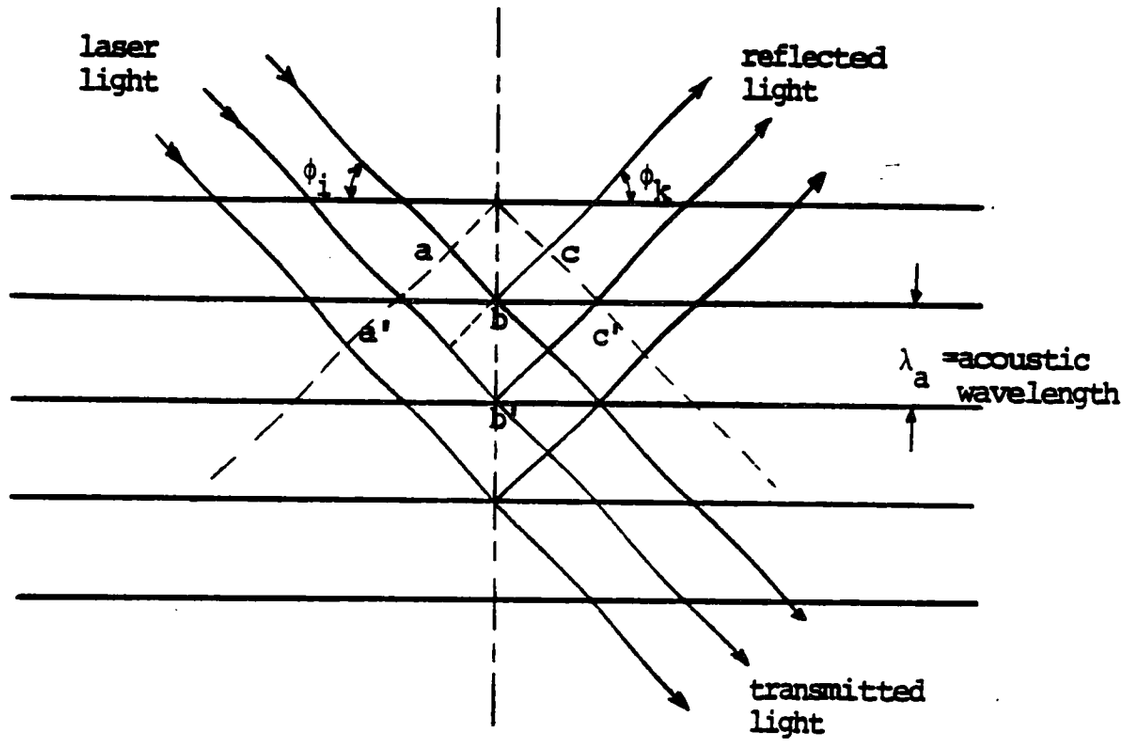


Fig. 4.1 *Reflections from an acoustic wave in a medium.*

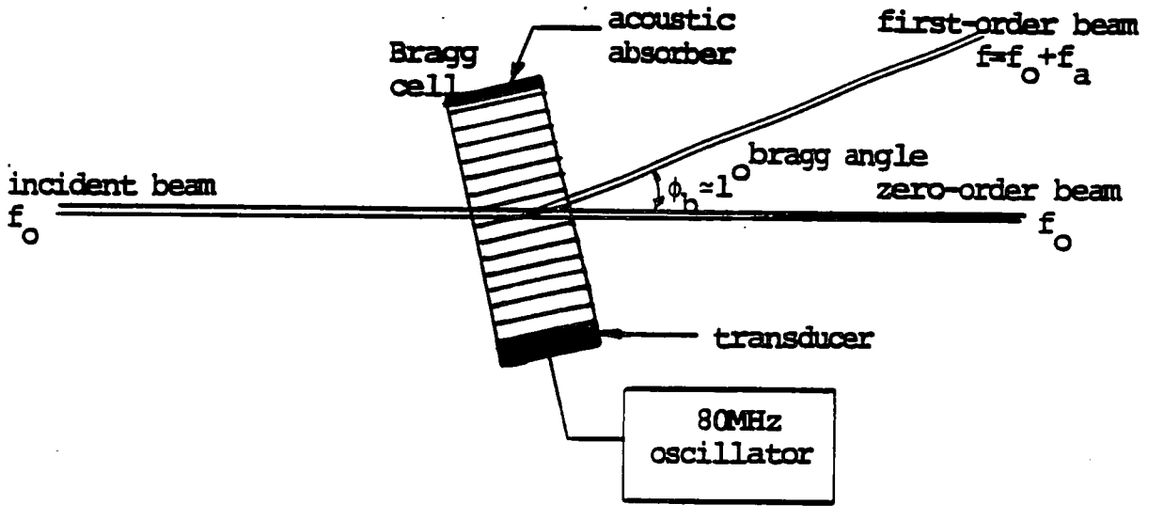


Fig. 4.2 *Bragg cell configuration for experiment, note the Bragg angle is exaggerated.*

### 4.1.B Electro-optic Crystal Modulator

In this section, a summary of the operation of an electro-optic modulator will be described. An attempt will be made to be brief since comprehensive discussions of electro-optic modulators and the particular modulator used for this experiment can be found in the thesis reports of J.R. Regazzi and R.T. O'Hara written for Lehigh University.[7,8] For more in depth information, the reader is referred to these papers.

The electro-optic modulator is based on the linear electro-optic effect (Poeckels effect). This effect causes the index of refraction of a suitable crystal to be linearly dependent upon an external electric field, specifically, the index of refraction will change at the modulation rate of the electric field. A 'suitable crystal' has optical characteristics of a crystal when there is no external field, i.e. it is birefringent, each direction of propagation has only two permissible polarizations of light which are mutually perpendicular and travel at different phase velocities. The velocities are given by $n_o$ and $n_e$, the ordinary and extraordinary indices of refraction. When an external field is applied, $n_o$ and $n_e$ are slightly changed in proportion to the field. Generally the two changes are different. Thus, a linearly polarized light beam incident upon such a crystal is split into mutually perpendicular components dependent upon the orientation of the birefringent axes.

Each component will see a different refractive index and thus travel at different velocities, resulting in relative phase retardation which is proportional to the applied electric field.

Fig. 4.3 is a schematic diagram showing how amplitude modulation is achieved by phase retardation in an electro-optic crystal modulator. The input light wave to the crystal can be considered to split into two component fields given by $E_{xi}$ and $E_{yi}$ as shown in Fig. 4.4. Note, the wave is travelling in the z-direction. The fields are given in general by

$$E_{xi} = \frac{E_i}{\sqrt{2}} \sin(\omega t - \beta_x z) \quad \text{and} \quad E_{yi} = \frac{E_i}{\sqrt{2}} \sin(\omega t - \beta_y z) \tag{4.6}$$

where $\beta_x z$ and $\beta_y z$ are the phase delays produced by the different indices of refraction of the ordinary and extraordinary rays. At the output of the crystal, the field is given by

$$E_0 = (E_{x0} + E_{y0})/\sqrt{2} \tag{4.7}$$

where $E_{x0}$ and $E_{y0}$ are the respective field components in the x and y directions at the output. Assuming no attenuation through the crystal, the output is given by:

$$E_o = \frac{E_i}{2} [\, \sin(\omega t - \beta_x z_0) + \sin(\omega t - \beta_y z_0) \,] \tag{4.8}$$

where the output is defined at $z = z_0$. But this output is oriented in the same direction as the input and with the output polarizer 90° from the input - there will be no output after

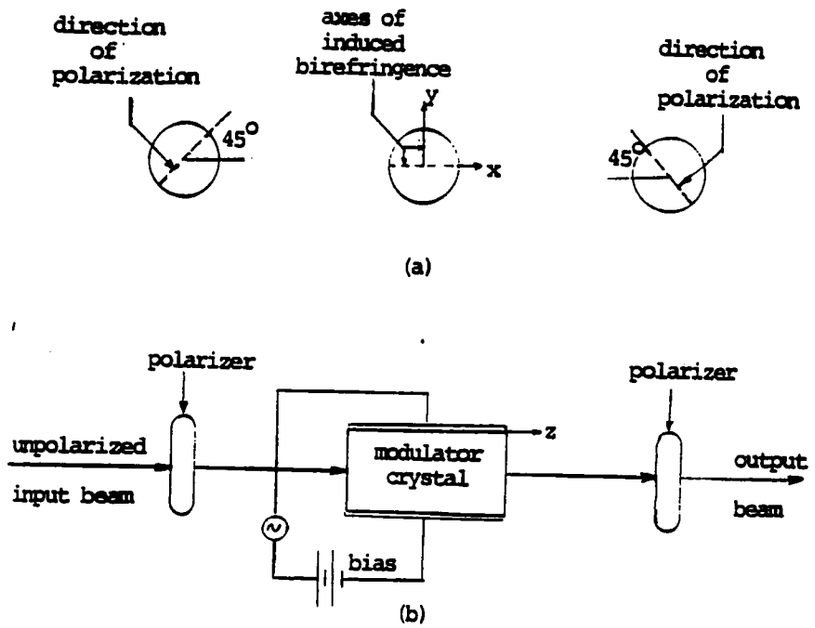


Fig. 4.3 *Amplitude modulation by phase retardation. (a) polarization planes of the polarizers and the induced electro-optic axes of the crystal. (b) optical set-up.*

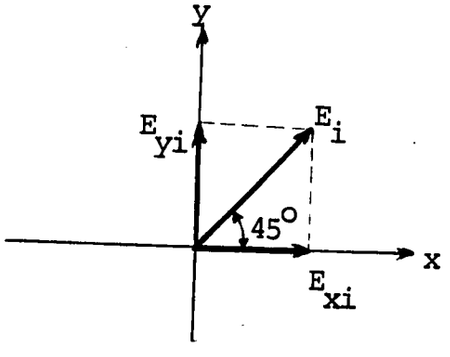


Fig. 4.4 *Input fields of light wave entering crystal.*

the polarizer. Maximum output will occur when the phase retardation of one component, for example $E_x$, is 180° from input to output. In this case, $E_x$ is negative from the chosen input reference and 4.8 becomes

$$E_0 = \frac{E_i}{2} \left[ -\sin(\omega t - \beta_x z_0) + \sin(\omega t - \beta_y z_0) \right] \quad . \tag{4.9}$$

Letting $\beta_x z_0 = \theta + \Gamma/2$, $\beta_y z_0 = \theta - \Gamma/2$, and $t' = t - \theta/\omega$ and using trigonometric operations 4.9 takes the form:

$$E_0 = E_i \sin(\Gamma/2) \cos\omega t' \quad . \tag{4.10}$$

The intensity of the output light is proportional to the square of the field:

$$N = N_i \sin^2(\Gamma/2) \cos^2\omega t' \quad . \tag{4.11}$$

The presence of the $\cos^2\omega t'$ term indicates that at most half-power on the average will be passed through the cross polarizer. Letting $N_0$ be the maximum output, 4.11 becomes

$$N = N_0 \sin^2(\Gamma/2) \quad . \tag{4.12}$$

The above discussion has been a simple derivation of the static modulation curve (4.12). For briefness, results from O'Hara's thesis will be used here. Considering $\Gamma$ as the phase shift between ordinary and extraordinary waves and $\omega_m$ as the modulating frequency, it was found that Eq. 4.12 could be written in the following form:

$$\frac{N}{N_0} = \sin^2\left( \frac{M\pi}{2} \sin\omega_m t + B\pi \right) \tag{4.13}$$

where M and B are defined in Fig. 4.5. Note that the nomenclature used here is taken from Eq. (7) of Dr. Eberhardt's Summary in the report titled "A Study of CW - LIDAR"[9].

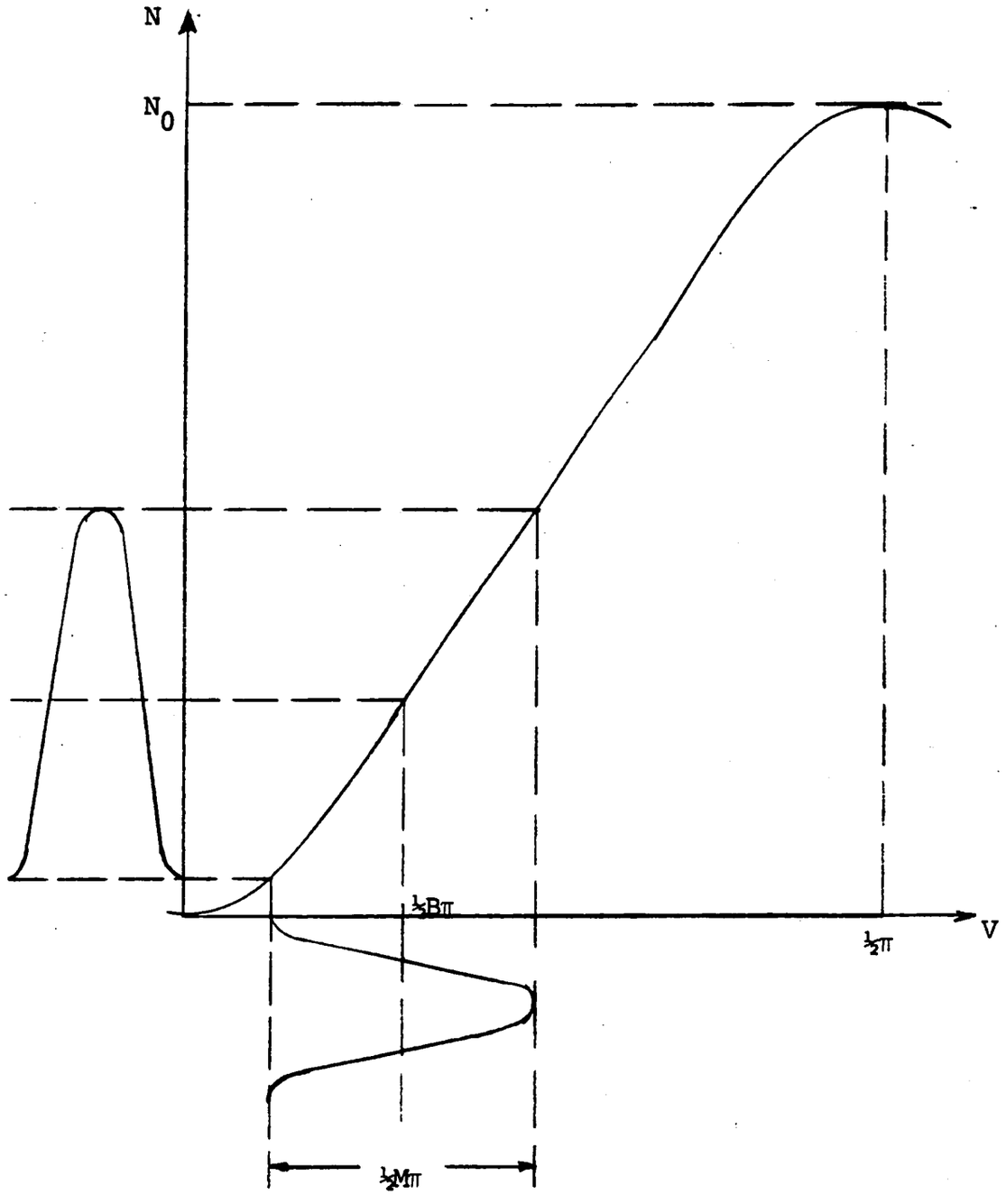


Fig. 4.5 *Nonlinear modulation process.*

If the bias coefficient, B, is equal to ½ which would require biasing at V = (¼)π and the modulation coefficient, M, is equal to 1, then 100% modulation is achievable between N = $N_0$ and N = 0. This is how the modulator is used in the system described in section 4.3. Note that for this case, the output is approximately linearly modulated at the input modulation frequency.

As a final note, the electro-optic crystal modulator will be used to demodulate the signal. Physically, the process of demodulation is accomplished the same way as modulation in the crystal, except that demodulation generates high frequency components which must be filtered out. Analytically, modulation and demodulation are accomplished by multiplication of a sinusoid. Thus the Bragg cell will be used to modulate the laser light and the electro-optic modulator will be used to demodulate the optical signal.

## 4.2 Derivation of Frequency Components

As described in section 2, a probe for which a carrier frequency is impressed on the light beam results in the most versatile system but also the most complex electronics. Because of this disadvantage, it was decided to optically demodulate the beam using the electro-optic modulator and thus reduce the complexity of the detection electonics. The Bragg cell is used

to modulate the beam and the electro-optic modulator to demodulate the beam. Since these two devices are approximately linear, simple modulation theory is used.

### 4.2.A. Light Intensity after Bragg Cell Modulation

For the optical system described in this report, it was decided to use the zero-order beam from the Bragg cell as the signal beam and the first-order beam as the reference. This choice was made to simplify construction of the optical system. Based on this decision, p and q are set to 0 and +1 in equation 2.1. Also, for this type of probe $\delta_r = 0$. Thus eq. 2.1 can be written to reflect this particular system:

$$S_d=\alpha_s S \exp i[k\{L_s+\delta_s \sin(\omega_s t+\theta_s)\}-\omega_0 t] \qquad (4.14)$$

$$R_d=\alpha_r R \exp i[kL_r-(\omega_0+\omega_b)t]$$

where all parameters have the same definition as given for eq. 2.1, except $\omega_b$ can now be interpreted as the Bragg cell frequency. After the signal and reference beams have been combined, the light intensity is given by:

$$N_d \propto (S_d + R_d)(S_d^* + R_d^*) \qquad (4.15)$$

Replacing eqs. 4.14 into 4.15, multiplying through, and using simple trigonometric identities, eq. 4.15 becomes

$$N_d \propto \alpha_s^2 S^2+\alpha_r^2 R^2+2\alpha_s\alpha_r SR\cos[\omega_b t+\phi+k\delta_s \sin(\omega_s t+\theta_s)] \qquad (4.16)$$

where $\phi=k(L_s-L_r)$.

Using trigonometric product relations, the last term in eq. 4.16

can be written in the following form:

$$\cos[\omega_b t+\phi+k\delta_s \sin(\omega_s t+\theta_s)]= \tag{4.17}$$
$$\cos\phi[\cos\omega_b t\cdot\cos(k\delta_s\sin(\omega_s t+\theta_s))-\sin\omega_b t\cdot\sin(k\delta_s\sin(\omega_s t+\theta_s))]$$
$$-\sin\phi[\sin\omega_b t\cdot\cos(k\delta_s\sin(\omega_s t+\theta_s))+\cos\omega_b t\,\sin(k\delta_s\sin(\omega_s t+\theta_s))].$$

At this point, an expansion formula must be introduced. For small x, the following Fourier series can be written

$$\cos(x\sin\theta) = J_0(x) + 2J_2(x)\cos2\theta + 2J_4(x)\cos4\theta + \cdots \tag{4.18}$$
$$\sin(x\sin\theta) = 2J_1(x)\sin\theta + 2J_3(x)\sin3\theta + \cdots .$$

Since it is desired to use the probe to measure small vibrations, then $\delta_s$ is small and eqs. 4.18 can be used in eq. 4.17. Thus eq. 4.17 becomes

$$N_d \propto \alpha_s^2 S^2+\alpha_r^2 R^2+2\alpha_s\alpha_r SRJ_0(k\delta_s)[\sin\phi\cdot\sin\omega_b t+\cos\phi\cdot\cos\omega_b t]$$
$$+2\alpha_s\alpha_r SRJ_1(k\delta_s)[\sin\phi\{\sin((\omega_b+\omega_s)t+\theta_s)+\sin((\omega_b-\omega_s)t-\theta_s)\}$$
$$-\cos\phi\{\cos((\omega_b-\omega_s)t-\theta_s)-\cos((\omega_b+\omega_s)t+\theta_s)\}] . \tag{4.19}$$

The higher order terms have been neglected since the higher order Bessel functions become very small with a small argument.

Using eq. 4.19 the power in each of the frequency components can be found. The power is proportional to the amplitude squares, for example, the power in the carrier frequency component is given by

$$P_c \propto [2\alpha_s\alpha_r SRJ_0(k\delta_s)]^2[(\sin\phi)^2+(\cos\phi)^2]=4\alpha_s^2\alpha_r^2 S^2R^2J_0^2(k\delta_s). \tag{4.20}$$

Similarly, the power in each of the sidebands is

$$P_{sb} \propto 4\alpha_s^2\alpha_r^2 S^2R^2J_1^2(k\delta_s) . \tag{4.21}$$

Before proceeding to demodulation of this signal, it is noteworthy that the power in the frequency components is independent of $\phi$ which represents the pathlength difference between the signal and reference beams without object vibration. This is a surprising and advantageous result since this implies that extreme precision is not necessary in the physical optical set-up in terms of pathlengths. Also, note that this result corresponds to Table 2.1 which states that the output signal is independent of optical phase for probe type 5.

### 4.2.B. Envelope Heterodyning

The term *envelope heterodyning* is used to describe the process of a modulated light beam sent through a second modulator at a slightly different modulation frequency, $\omega_m$. This process could also be called demodulation but is more properly described by envelope heterodyning.[9] The output will have an amplitude modulated component at the difference frequency, $\omega_b - \omega_m$.

The second modulator is implemented with the electro-optic modulator operated in its linear region. Recall that the electro-optic modulator has a modulation characteristic described by:

$$\sin^2\left(\frac{M\pi}{2}\sin\omega_m t + B\pi\right) \quad , \tag{4.22}$$

where $\omega_m$ is the modulating frequency. Using simple modulation theory, the frequency response of the signal described in eq. 4.19 is found by multiplying eq. 4.19 by eq. 4.22. Carrying out

the multiplication and using trigonometric product relations, the following expression is derived for the light intensity after envelope heterodyning:

$$
\begin{aligned}
N_{d(eh)} \propto\ & \frac{X}{2} - \frac{X}{2}\cos B\pi \cdot J_0\left(\frac{M\pi}{2}\right) + X \sin B\pi \cdot J_1\left(\frac{M\pi}{2}\right)\sin\omega_m t \\
& + Y(\sin\phi \sin\omega_b t + \cos\phi\cos\omega_b t)\left(1 - \cos B\pi \cdot J_0\left(\frac{M\pi}{2}\right)\right) \\
& + 2Y \sin B\pi \cdot J_1\left(\frac{M\pi}{2}\right)\{\sin\phi[\cos(\omega_m-\omega_b)t - \cos(\omega_m+\omega_b)t] \\
& \qquad + \cos\phi[\sin(\omega_m+\omega_b)t + \sin(\omega_m-\omega_b)t]\} \\
& + Z\{\sin\phi[\sin((\omega_b+\omega_s)t+\theta_s)+\sin((\omega_b-\omega_s)t-\theta_s)] \\
& \quad -\cos\phi[\cos((\omega_b-\omega_s)t-\theta_s)-\cos((\omega_b+\omega_s)t+\theta_s)]\}\left(1-\cos B\pi \cdot J_0\left(\frac{M\pi}{2}\right)\right) \\
& + Z \sin B\pi \cdot J_1\left(\frac{M\pi}{2}\right)\sin\phi\{\cos((\omega_m-\omega_b-\omega_s)t-\theta_s)-\cos((\omega_m+\omega_b+\omega_s)t-\theta_s) \\
& \quad +\cos((\omega_m-\omega_b+\omega_s)t+\theta_s)-\cos((\omega_m+\omega_b-\omega_s)t-\theta_s)\} \\
& + Z \sin B\pi \cdot J_1\left(\frac{M\pi}{2}\right)\cos\phi\{\sin((\omega_m+\omega_b-\omega_s)t-\theta_s)+\sin((\omega_m-\omega_b+\omega_s)t+\theta_s) \\
& \quad -\sin((\omega_m+\omega_b+\omega_s)t+\theta_s)-\sin((\omega_m+\omega_b-\omega_s)t-\theta_s)\} \qquad (4.23)
\end{aligned}
$$

where $X = (\alpha_s{}^2 S^2 + \alpha_r{}^2 R^2)$

$Y = \alpha_s \alpha_r SRJ_0(k\delta_s)$

and $Z = \alpha_s \alpha_r SRJ_1(k\delta_s)$ .

The above lengthy equation was included to show <u>all</u> the frequency components in the modulated light beam after passing through the electro-optic modulator. This is based on truncation of the series expansion, more components of small amplitude arise if higher order terms are included. It is necessary to determine which frequency components contain the desired information and are useful. This can be obtained by developing the frequency spectrum. The frequency spectrum after the Bragg

cell modulation is shown in Fig. 4.6, where a ratio between the amplitudes of the carrier frequency ($f_b$) component and either of the sidebands ( $f_b+f_s$ or $f_b-f_s$) will result in the desired information. Note that the information is in a high frequency range, approximately $f_b$ = 80 MHz, for which a sensitive photodetector is hard to find. After passing through the electro-optic modulator, in one of the components the information is shifted down by $f_m$, as shown in Fig. 4.7. Though higher frequency components also are generated, all of the information needed is contained in the spectrum shown in Fig. 4.7. In practice, the high frequency components are filtered out. From Fig. 4.7, it is easily recognized that the desired information can be found from a ratio of the amplitudes of the $f_m-f_b$ component and the $f_m-f_b-f_s$ (or $f_m-f_b+f_s$) component.

Using eq. 4.23 the power in these frequency components are readily found. The power in the $f_m-f_b$ component is given by:

$$P_{m-b} \propto A[2\alpha_s\alpha_r SRJ_1(\tfrac{1}{2}\cdot M\pi)\sin B\pi \cdot J_o(k\delta_s)]^2 \qquad (4.24)$$

and similarly, the power in either of the sidebands is:

$$P_{\substack{m-b-s \\ (m-b+s)}} \propto A[\alpha_s\alpha_r SRJ_1(\tfrac{1}{2}\cdot M\pi)\sin B\pi \cdot J_1(k\delta_s)]^2 \quad . \qquad (4.25)$$

Since $\delta_s$ is small, then $J_0(k\delta_s)\simeq 1$ and the power ratio is found to be

$$\frac{P_{m-b-s}}{P_{m-b}} = \frac{[J_1(k\delta_s)]^2}{4} \quad . \qquad (4.26)$$

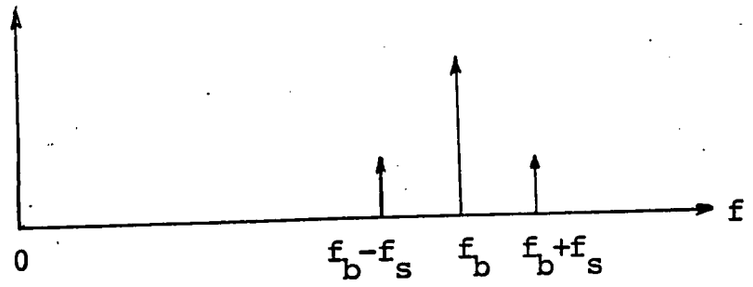


Fig. 4.6 *Frequency spectrum after Bragg cell modulation.*

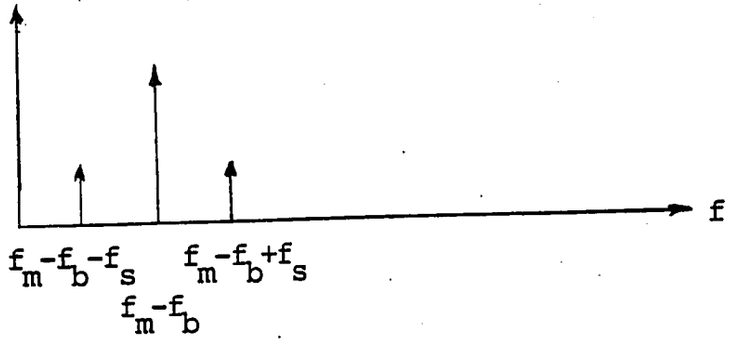


Fig. 4.7 *Frequency spectrum after the crystal modulator.*

In eqs. 4.24 and 4.25, 'A' is the attenuation of the electro-optic modulator.

The surprisingly simple result in eq. 4.26 leads to a straightforward detection process to find $\delta_s$. After the beam has passed through the electro-optic modulator, a photodetector must be used to convert the signal to electric current. If $\omega_m$ is chosen to be within a close proximity of $\omega_b$, then the information is in a low frequency range. Thus, a photomultiplier can be used since it is efficient with a low noise level at low frequencies. The detection electronics will be discussed further on in the report, but for now it will suffice to state that the frequency components needed are readily filtered out. The power in these components, $P_{m-b}$ and $P_{m-b-s}$, are proportional to the detected current.

Recognizing that for $x < 0.4$ the following equation is accurate to two decimal places

$$J_1(x) \simeq x/2 \tag{4.27}$$

and letting $k = 2\pi/\lambda_0$ where $\lambda_0$ is the laser wavelength, the following equation for $\delta_s$ is derived:

$$\delta_s = \frac{2\lambda_0}{\pi} \left( \frac{P_{m-b-s}}{P_{m-b}} \right)^{\frac{1}{2}} . \tag{4.28}$$

Note that a table could just as well have been used to find $J_1(k\delta_s)$ but $\delta_s$ is small enough to justify using eq. 4.27.

The above derivation has proved that theoretically a small

surface vibration is detectable using an optical heterodyne system. By also using envelope heterodyning, the result in eq. 4.28 shows only two measurements need to be made, specifically, the power at the difference frequency and its sideband. A complete description of the optical system and related electronics follows directly in section 4.3.

## 4.3 Description of Optical System and Detection Electronics

Based on the discussion in section 2 of a general optical heterodyne system and the description of special optical components and the theory of optical heterodyning developed in sections 4.1 and 4.2, the optical set-up can now be drawn, see Fig. 4.8.

### 4.3.A. Optical System

The Bragg cell is powered by an 80 MHz oscillator which is monitored by a frequency counter. The cell modulates the incoming laser light and thus produces the zero-order and first-order beams which are used for the signal and reference beams, respectively. In order for the first-order beam to be modulated exactly by the acoustic frequency (eq. 4.5), the cell must be tilted at the Bragg angle.

The lens is used to focus the signal beam onto the test object to assure the coherence of the speckle field at the

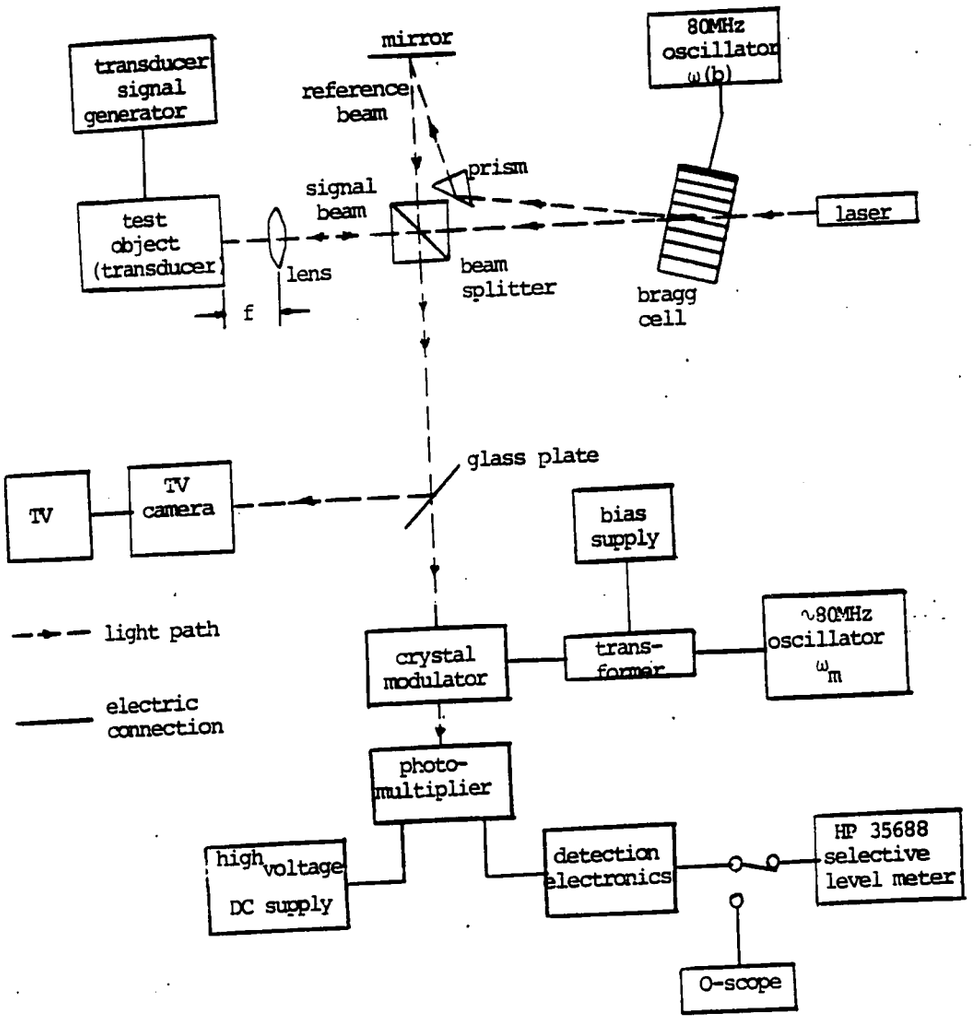


Fig. 4.8 *Optical set-up.*

detector, as discussed in section 3. The two beams are then superimposed at the beamsplitter. An effort was made to make the pathlengths approximately equal, but as shown earlier, the pathlengths are not critical.

A small portion of the superimposed light beam is reflected by a glass plate and is directed to a TV camera. The purpose of the TV camera is two-fold. The TV screen allows viewing of the speckle field and permits focusing the signal beam onto a section of the test object where the speckles appear to be larger and more well-defined. Larger speckles are desirable because it facilitates detection within a single speckle where the light is coherent. Viewing of the signal and reference fields on the TV screen also provides a simple way of adjusting the light intensity of the beams. This is accomplished by varying the power provided to the Bragg cell. It is desirable to have the intensities of the two fields equal. Consider that the total intensity is normalized to 1.0 and recalling that the power in each of the frequency components is proportional to $\alpha_s S \alpha_r R$, then the maximum power theoretically obtainable in each of these components will occur when $\alpha_s S = \alpha_r R = 0.5$. Note, from the result given in eq. 4.28, the actual values for $\alpha_s S$ and $\alpha_r R$ are unnecessary but more power present at the detector results in easier detection.

After the glass plate, the light beam passes through the

electro-optic modulator. The crystal itself has the dimension of only 0.5 mm for both the height and width. This aids in focusing on a single speckle for detection. To produce the electro-optic modulation effect, the crystal is excited with a high power signal generator. The transformer presents a signal three times the amplitude produced by the signal generator. This allows operation of the generator at lower, more manageable power levels. The modulation frequency for the crystal, $f_m$, is set to be approximately 80 MHz which is the Bragg cell frequency and is monitored with another frequency counter. A bias supply is included in the circuit to control the bias level which determines the region of operation on the static modulation curve for the crystal. A complete and thorough description of the electro-optic modulator and its operation can be found in the thesis by R.T. O'Hara written for Lehigh University[8].

The photomultiplier tube is placed immediately following the electro-optic modulator. It is powered by a high voltage variable DC supply. If the incoming light level is low, the voltage may be increased to enhance the amplification in the photomultiplier. But an increase in the applied voltage results in an increase in the dark current causing additional noise. Thus an optimum applied voltage must be used which allows a

minimum noise level while providing a substantial amplification.

This concludes the description of the optical system. Procedures for operating the system will be presented in section 6.

### 4.3.B. Detection Electronics

The detection electronics are rather uncomplicated. The requirements for the circuit are as follows,

(1) protection against a high DC voltage from the photomultiplier,

(2) ability to measure the DC photomultipler current,

(3) a low DC output level, approximately 1 V, to protect the oscilloscope,

(4) a low pass filter with a good frequency response,

and

(5) small output capacitance and an output impedance of approximately 50 ohms in order to match both the oscilloscope and the receiver.

It was chosen to use an op amp in the low pass filter because of its small output resistance, small output capacitance, and good frequency response. An output stage is added which allows matching to the oscilloscope and the receiver. Note, only one or the other may be connected at a time since matching between three terminals is impossible.

Considering the requirements and considerations described above, a circuit diagram can be drawn for the detection electronics, see Fig. 4.9. Considering the simplicity of the circuit, further discussion is unnecessary.

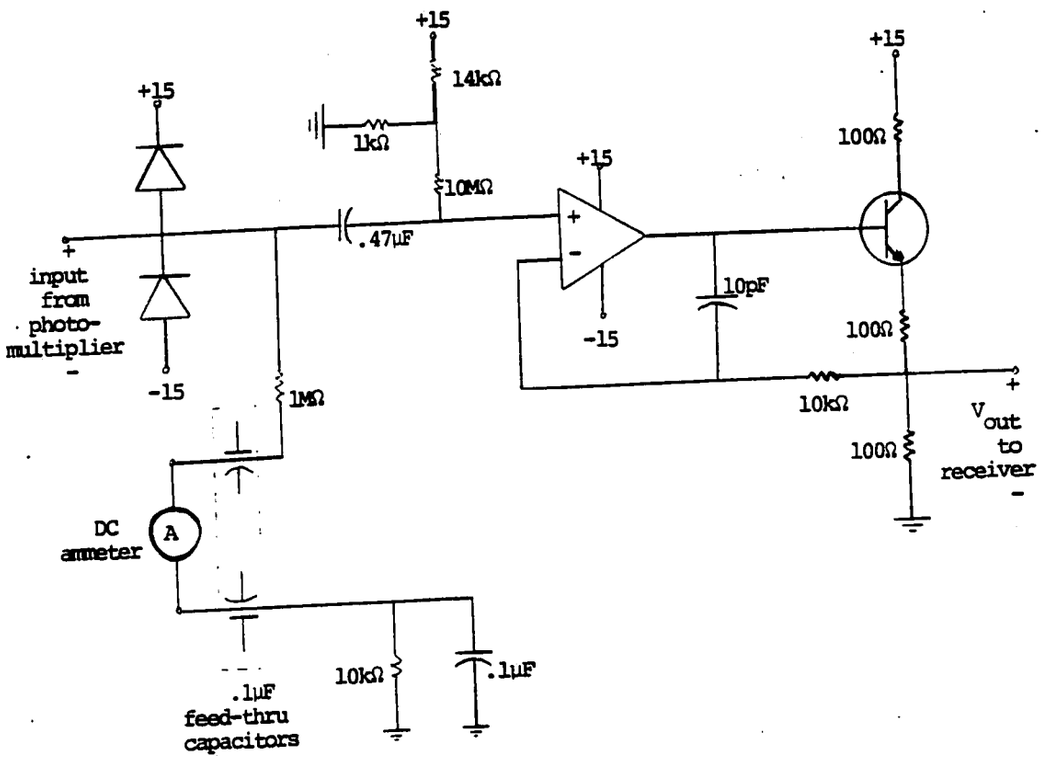


Fig. 4.9 *Detection electronics.*

## 4.4 Concluding Remarks

Section 4 has presented necessary information concerning special optical components, specifically, the Bragg cell and the electro-optic modulator, and developed the theory of optical heterodyning which lead directly to the physical optical system and related electronics. The result given in eq. 4.28 implies that, if the system is adjusted and working properly, only two measurements are necessary to find the small amplitude of vibration, $\delta_s$.

At this point, a couple of remarks are necessary concerning material which has not been considered here. Beam misalignment was not addressed but was a serious consideration in the laboratory. If the signal and reference beams are not aligned at the detector, the power in the carrier and sideband components is reduced by a factor of

$$\sin^2(2kD_b\sin\alpha)/(2kD_b\sin\alpha)^2 \qquad (4.29)$$

where $2\alpha$ is the angle at which the two beams are inclined to one another, $2D_b$ is the width of either the beam or the detector depending on which is smaller, and $k = 2\pi/\lambda$.[1] Choosing $2D_b$=0.5 mm (width of the crystal) and $\lambda$ = 633 nm (laser wavelength), for $2\alpha = 0.05°$ the degradation factor is 0.14 but for $2\alpha = 0.005°$ the degradation factor is 0.98. This demonstrates that careful alignment is necessary and in the laboratory much time and effort was devoted to precise alignment of the beams. The

degradation factor given in eq. 4.29 is derived in Reference 1 and therefore the derivation was not included here. Note that the degradation factor is the same for the carrier and the side-band and thus does not affect the ratio used to determine the amplitude of vibration, but it does reduce the power in the signal and therefore affects the signal - to - noise ratio. Therefore, the effect of beam misalignment will be considered in order to find the signal - to - noise ratio (section 5).

Another factor that was not discussed for the detection electronics is the bandwidth of the low pass filter. Originally, it was thought that a wide bandwidth would be desirable but it was realized that a smaller bandwidth would facilitate measurement of the separate frequency components. The reason for this will become evident in section 6 which will explain the method of measurement.

In conclusion, all aspects of the system have been addressed. Theory predicts that the system design will work if there is sufficient power in the signal. This leads to the next section which discusses sensitivity and signal - to - noise ratios.

# 5. Noise and Sensitivity Considerations

If one neglects the problems of beam misalignment, optical pathlength variations, and diffraction effects then all of the probes in Table 2.1 demonstrate little difference in their inherent sensitivity. However, they are differentiated when consideration is given to system noise and other effects which attenuate the signal power. In the system described in section 4, optical pathlength variations were of no concern but beam misalignment may cause a notable reduction of signal power. Diffraction effects may be neglected when the optical beam spot size at the surface is sufficiently small compared with the acoustic wavelength. Since this is the case, then the neglecting of diffraction effects is justified.

For an optical homodyne system, where optical pathlength variations are critical, special care must be exercized to assure the proper lengths or complete loss of signal may occur. Beam misalignment is of concern here also.

These considerations are discussed at length in this section. The theory of noise is presented and the signal - to - noise ratio is developed for a number of special related cases.

## 5.1 Theory of Noise

In optical systems, the major source of noise is generally found in the photodetector. Other sources of noise such as

fluctuations in the laser output, atmospheric turbulence, and frequency noise of the acoustic sources are justifiably neglected.[9] The photodetector to be used is a photomultiplier. In simple terms, the photomultiplier consists of a photocathode, a dynode chain, and an anode. The photoelectrons produced by the photocathode (similar to photoelectric cells) are focused onto the first dynode. Low noise amplification is achieved by secondary emission of electrons in the dynode chain. The anode forms the end of the chain which *collects* the electrons that originate from the cathode and are *multiplied* by each dynode stage.

Noise from the photomultiplier is principally shot noise, that is background and amplifier noise can be neglected. The principal cause of this noise is thermionic emission from the cathode and also to a smaller extent from the first dynode in the photomultiplier.[10] Though there is only a small amount of noise contributed by the rest of the photomultiplication process, instead of neglecting it, a degradation factor may be included which accounts for the additional noise.

The photocurrent at the cathode is

$$I(t) = \frac{q_e e}{h\nu} N(t) \tag{5.1}$$

where $q_e$ is the cathode quantum efficiency, e is the electronic charge, $h\nu$ is the photon energy, and N(t) is the instantaneous light power. The noise in the photomultiplier causes a fluctu-

ation in the cathode current, this is termed the *dark current* and is represented by:

$$\overline{i^2} = \frac{2q_e e^2 a^2}{h\nu} \overline{N}\Delta f \quad , \tag{5.2}$$

where $\overline{i^2}$ is the mean square deviation, $\overline{N}$ is the average light power, a is the degradation factor, and $\Delta f$ is the post detection bandwidth. Equations 5.1 and 5.2 can be used to form the signal - to - noise power ratio:

$$\frac{I^2_{rms}}{\overline{i^2}} = \frac{q_e}{2h\nu a^2 \Delta f} \frac{N^2_{rms}}{\overline{N}} \quad . \tag{5.3}$$

Equation 5.3 is a general result for any optical system employing square law detection with a photodetector for which the dark current is the principal cause of excess noise. The following discussions will utilize this result to find the signal - to - noise ratios for the optical systems of interest.

## 5.2 SNR - Optical Heterodyne Technique

The signal - to - noise ratio for the system described in section 4 will be found first. Initially, only the attenuation of the signal and reference beams, and the electro-optic modulator will be included. Then other factors will be considered, such as beam misalignment and speckle size.

For the optical heterodyne technique, $\overline{N}$ and $N^2_{rms}$ are readily found from equations 4.23 and 4.25, respectively. $N^2_{rms}$ is the light power in the signal beam and $\overline{N}$ is the average (DC)

light level:

$$N^2_{rms} = (\alpha_s S)^2 (\alpha_r R)^2 \cdot J_1^2(\tfrac{1}{2} \cdot M\pi) J_1^2(k\delta_s) \quad (5.4)$$

and $$N = \tfrac{1}{2}[(\alpha_s S)^2 + (\alpha_r R)^2] \cdot [1 - \cos B\pi \cdot J_0(\tfrac{1}{2} \cdot M\pi)] \quad . \quad (5.5)$$

Replacing the above equations into eq. 5.3 yields the following result for the signal - to - noise ratio:

$$\frac{I^2_{rms}}{\bar{i}^2} = \frac{q_e A}{h\nu a^2 \Delta f} \frac{(\alpha_s S)^2 (\alpha_r R)^2 J_1^2(\tfrac{1}{2} \cdot M\pi) J_1(k\delta_s)}{[(\alpha_s S)^2 + (\alpha_r R)^2] \cdot [1 - \cos B\pi \cdot J_0(\tfrac{1}{2} \cdot M\pi)]} \quad (5.6)$$

where the term 'A' accounts for the attenuation in the electro-optic modulator.

The result given in eq. 5.6 is not very revealing, therefore it is worthwhile to investigate a special case. From light power measurements made in the laboratory and information from Dr. Eberhardt's summary[9], the attenuation in the electro-optic modulator can be found. The power levels of the signal and reference beams directly before the electro-optic modulator were measured to be .24 μW and 86 μW, respectively. Thus $(\alpha_s S)^2 = 0.24$ μW and $(\alpha_r R)^2 = 86$ μW. 'A' can be determined from the incident light power level on the modulator and information given on pages 28 and 29 in Dr. Eberhardt's section of A Study of CW - LIDAR[9]: refer to Table 5.1. The values in Table 5.1 merit further explanation. Between (1) and (2), 3 dBm are lost in the input polarizer since the incident light is unpolarized. (3) gives the fraction of the light incident on the crystal: the only useful light is that which covers the front

surface of the crystal but 0.12 μW is the power of the entire speckle field which had an approximate diameter of 5 mm. Therefore, the area of the beam is approximately 20 $mm^2$. The value given for (3) is calculated from:

$$(\text{value}(2))\,(0.25\ mm^2/20\ mm^2) = 0.12\ \mu W(.25/20) \qquad (5.7)$$
$$= 1.5\ nW\ ,$$

and is an approximated value of the speckle power on the crystal. The attenuation of 9.4 dBm between (3) and (4) was estimated from values in Dr. Eberhardt's report.

Now that A has been determined, a special case can be investigated to find the signal - to - noise ratio. The values which are used in equation 5.6 are given in Table 5.2.

By using the values in Table 5.2 and assuming a test object vibration of $\delta_s = 0.05\ \lambda_0$, the SNR was found to be 13.3 dB. This relatively low SNR is mainly due to two factors. One is the substantial loss of power in the reflected signal beam off the test object. The laser power output is 2.1 mW and after the Bragg cell, the signal beam is 1 mW. But, after the signal beam has been reflected from the test object and rejoined with the reference beam, the signal power is only 0.24 μW. This attenuation of 36.2 dBm can partially be accredited to loss in the beamsplitter and lens, but the largest portion of this loss is due to the scattering of the light upon reflection from a *rough* surface (*rough* compared to a mirror). The other inescapable factor is the attenuation of 31.4 dBm of the electro-optic modulator.

| | light power | attenuation |
|---|---|---|
| (1) incident signal beam | .24 μW | |
| (2) after first polarizer | .12 μW | } 3 dBm |
| (3) amount of useful light on crystal | 1.5 nW | } 19.04 dBm |
| (4) after crystal and second polarizer | .17 nW | } 9.4 dBm |
| total attenuation of electro-optic modulator (A) | | 31.44 dBm |

Table 5.1 *Attenuation of electro-optic modulator.*

| PARAMETER | VALUE |
|---|---|
| $(\alpha_s S)^2$ | .24 μW |
| $(\alpha_r R)^2$ | 86 μW |
| A | 31.44 dBm |
| M | 1.0 (100% modulation) |
| B | ½ |
| Δf | 7 kHz (BW of post-detection electronics) |
| a | 1.2 (common value of degradation factor) |
| $q_e$ | .05 (common value for quantum efficiency of photomultiplier at 632.8nm) |
| hν | $3.14\times10^{-19}$ (for $\lambda_0$=632.8nm) |

Table 5.2 *System parameters and their values.*

Other factors need to be considered in finding the SNR. It was assumed in the previous analysis that a single speckle was at least as large as the crystal face. If the test surface is rough enough this assumption may not hold. in which case eq. 5.7 must be modified. For example, if the area of a single speckle is only 0.125 $mm^2$ (covers half the crystal face), the amount of useful light on the crystal is approximately (0.12 μW)(0.125/20) = 0.75 nW and the SNR becomes 10.3 dB. For this report, the assumption that a single speckle is at least as large as the crystal face is valid and therefore, further discussion is presently irrelevant.

Another important factor affecting SNR is the beam misalignment. As stated previously, the power is degraded by a factor of

$$\sin^2(2kD_b\sin\alpha) \;/\; (2kD_b\sin\alpha)^2 \qquad (5.8)$$

where, in this case, $2D_b$ is the width of the crystal and $2\alpha$ is the angle that the signal and reference beams are inclined to one another at the crystal surface. If $2\alpha = 0.05°$, then the degradation factor is 0.141 and the SNR becomes -5.17 ! Evidently, the signal is in the noise and can not be detected. Naturally, if a higher power laser is used the signal level should be above the noise level. Since a higher power laser is not available it seems logical to investigate the possibility of placing a small mirror on the test surface to boost the signal beam power.

Using specular reflection, the assumption can be made that the signal and reference beam powers are approximately equal. Therefore, $(\alpha_s S)^2 = (\alpha_r R)^2 = 86\ \mu W$. Using all the same values as before, the signal - to - noise ratio becomes 35.87 dB. This is a much more acceptable value but beam misalignment has not been considered yet. The graph on the following page shows how the SNR is affected by beam misalignment. Specifically, for $2\alpha = 0.05°$, the signal - to - noise ratio is 27.4 dB versus -5.12 dB for the same angle without using specular reflection.

Therefore, theory predicts that with the laser power available the signal will be diffucult, if not impossible, to detect for the original system shown in Fig. 4.8, using individual speckles. But with specular reflection, good results can be expected.

## 5.3 SNR - Optical Homodyne Technique

It is of interest to compare the signal - to - noise ratio of the heterodyne technique to a comparable homodyne technique to justify the choice of the heterodyne technique. A comparable system is shown in Fig. 5.2. Using the same definitions of terms as before, the light level at the detector is found to be:

$$N_d \propto (\alpha_s S)^2 + (\alpha_r R)^2 + 2\alpha_s \alpha_r SR[\cos\phi J_0(k\delta_s) - 2\sin\phi J_1(k\delta_s)\sin(\omega_s t + \theta_s) + 2\cos\phi J_2(k\delta_s)\cos(2(\omega_s t + \theta_s))] \quad . \qquad (5.9)$$

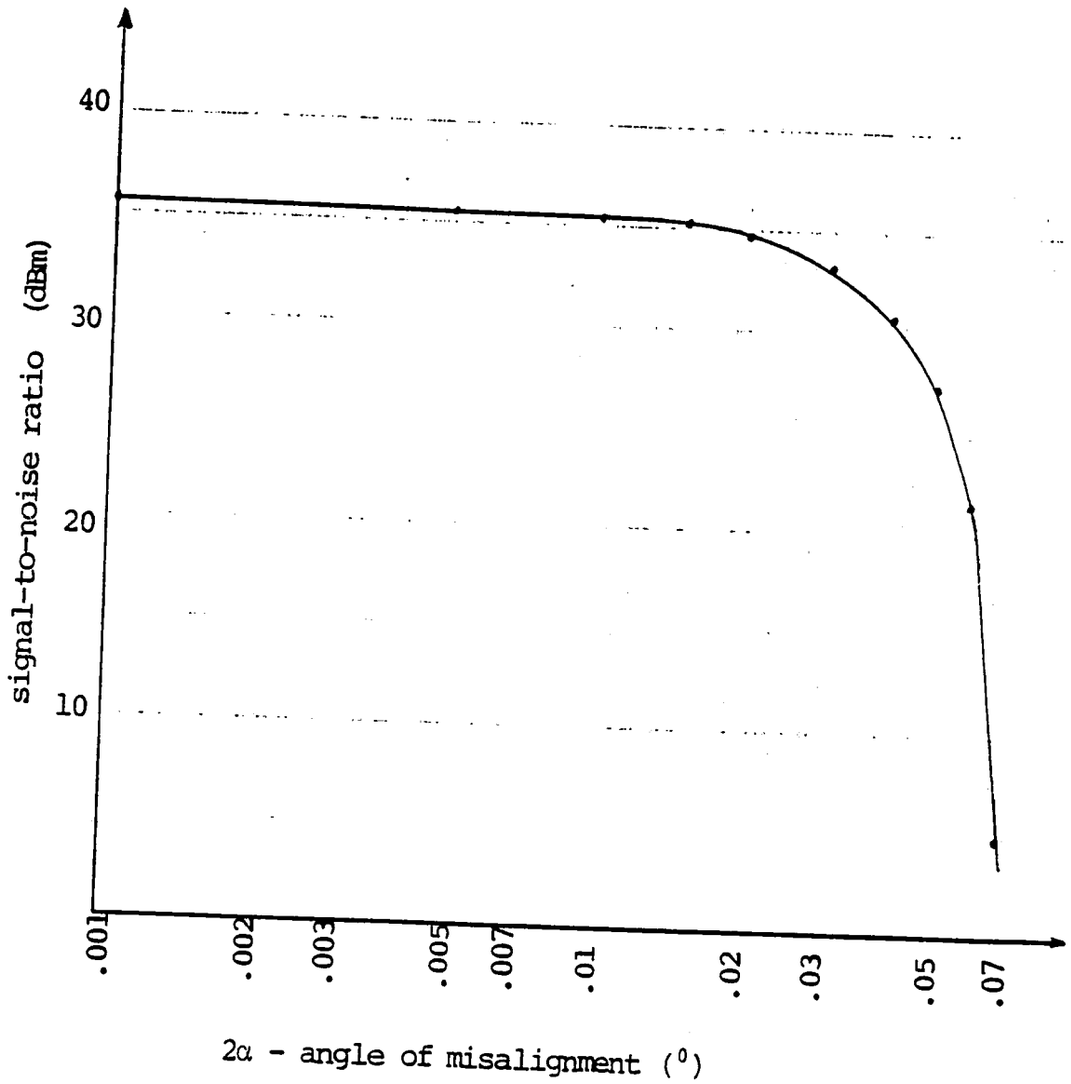


Fig. 5.1 *SNR vs. Angle of misalignment for the optical heterodyne technique using specular reflection.*

*Surface vibration* $\delta_s = 0.05\lambda_0$.

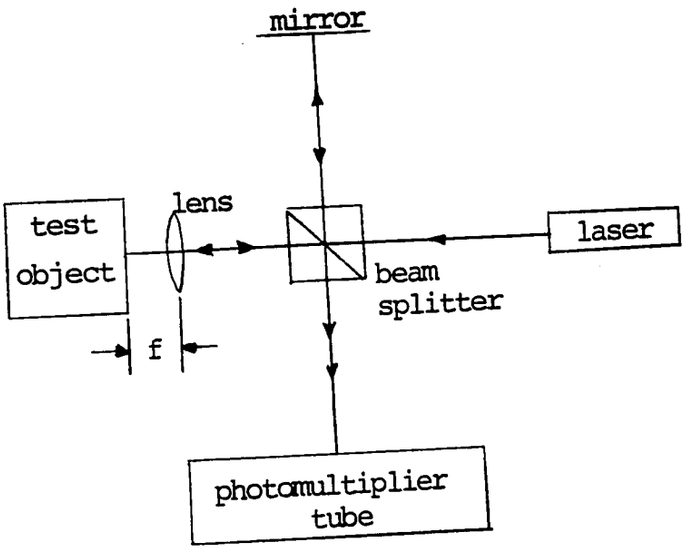


Fig. 5.2 *Basic optical homodyne system to be compared with optical heterodyne system.*

Note that all related derivations for this subsection can be found in appendix C.

From eq. 5.9, the quantities needed to find the signal - to - noise ratio are readily determined

$$N^2_{rms} = 16(\alpha_s S)^2(\alpha_r R)^2 \sin^2\phi J_1^2(k\delta_s) \tag{5.10}$$

and

$$\bar{N} = (\alpha_s S)^2 + (\alpha_r R)^2 + 2\alpha_s\alpha_r SR\cos\phi J_0(k\delta_s) \quad . \tag{5.11}$$

Using the above equations and eq. 5.3, the SNR is given by:

$$\frac{I^2_{rms}}{\bar{i}^2} = \frac{8q_e}{h\nu a^2\Delta f} \frac{(\alpha_s S)^2(\alpha_r R)^2 \sin^2\phi J_1^2(k\delta_s)}{[(\alpha_s S)^2 + (\alpha_r R)^2 + 2\alpha_s\alpha_r SR\cos\phi J_0(k\delta_s)]} \quad . \tag{5.12}$$

From calculations found in the appendix, 0.24 μW and 55.7 μW were approximated for $(\alpha_s S)^2$ and $(\alpha_r R)^2$, respectively. Initially, it is assumed that $\phi = k(L_s - L_r)$ is such to produce the maximum SNR. This occurs for $\sin^2\phi = 1.0$ which occurs when $(L_s - L_r) = n\lambda_0/4$ $(n = 1,3,\ldots)$. All the other values are the same as those used in the previous analysis, as tabulated in Table 5.2. The maximum SNR is calculated to be 58.7 dB. This seems rather discouraging since the SNR of the heterodyne system is 13.3 dB. This difference is easily explained. Due to the envelope heterodyning, the factor of 8 in eq. 5.12 is not included and a factor of $J_1^2(\frac{1}{2}\cdot M\pi)$ is included in the numerator. For M = 1.0, $J_1^2(\frac{1}{2}\cdot\pi) = 0.3207$ which results in a difference of 5 dB. The factor of 8 results in a difference of 9 dB. This brings the SNR down to 44.7 dB. The remaining difference of 31.4 dB is the attenuation of the electro-optic modulator as shown in Table 5.1.

Therefore, the reason that the signal - to - noise ratio of the heterodyne technique is so much less than the homodyne technique is completely due to the envelope heterodyning accomplished with the electro-optic modulator. So why is this technique preferable over the system shown in Fig. 5.2 ? The answer is that one important factor has not been considered yet... optical pathlength variations. Note the direct dependence of the SNR, given in eq. 5.12, on $\sin^2\phi$. If $(L_s-L_r) = 0$ then $\phi = 0$ and the signal dissappears ! The difference in a high SNR to a nonexistent signal is a pathlength difference of $\lambda_0/4$ which for HeNe laser light is only 158 nm. Therefore, the pathlengths of the signal and reference beams are critical and make optical adjustments a diffucult and tedious chore. Note that beam misalignment has not even been considered yet. The beam misalignment has the exact same degrading effect on the SNR as given in eq. 5.8.

In light of these diffuculties, it is realized that although a homodyne technique is very sensitive when adjusted properly, it does not lend itself to a practical, versatile, and flexible tool. Due to the critical optical pathlength dependence, one can imagine the diffuculties in testing different surfaces especially if the surface is immobile. The reference mirror would have to be used to adjust accurately for optical pathlength *and* beam misalignment, whereas it would only be needed

to align the beams in the heterodyne system which is a less tedious and critical process. Due to the independence of optical phase for the heterodyne technique, it more readily lends itself to testing different surfaces and testing in different environments other than the laboratory. Also, the homodyne technique can not measure the high frequency vibrations that the heterodyne technique is capable of. Considering these disadvantages, the optical heterodyne system proves itself to be a more practical tool and therefore was chosen over the homodyne system.

## 5.4 SNR - Concluding Remarks

The previous section presented the result that a heterodyne technique is much more practical than a homodyne technique. But it was also discovered that the second modulation causes a significant loss in the signal. It is of interest at this point to find the SNR without the envelope heterodyning.

Using eq. 4.19, $N^2_{rms}$ and $\bar{N}$ are readily found:

$$N^2_{rms} = 4(\alpha_s S)^2(\alpha_r R)^2 J_1^2(k\delta_s) \tag{5.13}$$

and

$$\bar{N} = (\alpha_s S)^2 + (\alpha_r R)^2 \quad . \tag{5.14}$$

Note that there is no dependence on optical pathlength variations. Again using eq. 5.3, the SNR is found to be:

$$\frac{I^2_{rms}}{\bar{I}^2} = \frac{2q_e}{h\nu a^2 \Delta f} \frac{(\alpha_s S)^2(\alpha_r R)^2 J_1^2(k\delta_s)}{[(\alpha_s S)^2 + (\alpha_r R)^2]} \quad . \tag{5.15}$$

Assuming that a detector is used which has the same quantum

efficiency as the photomultipler used in the previously discussed systems, then $q_e$ = 0.05 and all the other values are unchanged. The SNR for the optical heterodyne system without envelope heterodyning is 52.7 dB. Comparing this to the SNR of the homodyne technique, one notices that due to the heterodyning technique the factor of 8 in eq. 5.12 is reduced by a factor of 4. Thus, the SNR is 6 dB less than the maximum SNR for the homodyne technique. This fortifies the statement made at the beginning of this section that the probes oulined in Table 2.1 demonstrate little difference in their inherent sensitivity (note that there are no probes in Table 2.1 that use envelope heterodyning). Again, pathlengths are of no immediate concern and beam misalignment has the same effect.

If this heterodyne technique has a significantly higher SNR than the technique using envelope heterodyning, then why is the latter chosen over the former ? An important but impractical assumption was made to find the SNR = 52.7 dB. It was assumed that a detector is used with a quantum efficiency of 0.05. Knowing that the modulation frequency is 80 MHz (from Bragg cell), a detector is needed for which $q_e$ = 0.05 at the laser wavelength of $\lambda_0$= 632.8 nm with a modulation bandwidth of at least 80 MHz. This requirement is not so easily fulfilled. Furthermore, a detector with useful characteristics was not available for this experimentalist. An attempt was made to use

an avalanche photodiode with a preamplifier which was made available. Unfortunately, it operated optimally at .9 μm and a lower modulation frequency, 40 MHz would have been acceptable. Thus, detection with the photodiode would have been possible if a Bragg cell with a modulating frequency of 40 MHz was used, but only the 80 MHz Bragg cell was available. A quantitative discussion of detection using the avalanche photodiode for the optical heterodyne system without a second modulator is presented in the Results and Conclusions.

This section has explained why an optical heterodyne technique is preferable over a homodyne technique. Also, the optical heterodyne technique chosen includes demodulation since without the demodulation a photodetector with high modulation frequency capabilities is needed and, due to cost and inavailability, such a detector could not be obtained.

# 6. Procedure for Measurement of Surface Vibrations

To facilitate the discussion of procedure, a diagram of the system which resulted in the determination of a small surface vibration is shown in Fig. 6.1. Note that the diagram is simply a more in depth picture of the system shown in Fig. 4.8.

Assuming that all optical alignments have been completed, for proper operation of the system, a number of initial steps must be taken. The photomultipler DC supply is initially set to a relatively low voltage (∿500 V), this reduces the dark current. With all oscillators turned off, the polarizers must be adjusted so that polarizer 1 polarizes incoming light at a 45° angle and polarizer 2 is 90° from polarizer 1. With polarizer 1 set properly, setting polarizer 2 is accomplished by rotating the polarizer until there is almost no current reading on the ammeter. Note, it is impossible to get no current reading due to the dark current. After powering the Bragg cell and setting its frequency to 80 MHz, set to Bragg angle and adjust intensities of the signal and reference beams by adjusting the power of the 80 MHz oscillator and observing the effect on the TV screen. Adjust the bias of the crystal and observe the current level on the ammeter. Note the maximum and minimum currents. $I_{max}$ should not be greater than 15 μA since this would turn on one of the protection diodes (see Fig. 4.9). A maxi-

mum current level of approximately 10 - 12 μA is a good value and is set by adjusting the DC supply for the photomultipler: increasing voltage results in increasing current. The desired bias setting is in the middle of the static modulation curve, B = ½. This occurs when the current is $I_{avg} = (I_{max} + I_{min})/2$, which is 5 - 6 μA. With the bias set to zero, the $\omega_m$ oscillator is turned on and its amplitude adjusted to bring the current to $I_{avg}$. This method reduces the chances of overheating the crystal.

The modulating frequency, $\omega_m$, is set to be close to $\omega_b$, approximately 3 - 6 kHz away, and the carrier is viewed on the oscilloscope. If all the previous settings have been made correctly, close to 100% modulation should be achieved. This is checked on the oscilloscope by placing a chopping wheel in the optical path to see the zero and maximum light levels. 100% modulation is achieved when the minimum value of the trace corresponds exactly with the zero DC light level. At this point, adjustments are made to approach 100% modulation as closely as possible.

When the preparation is complete, the system output is connected to the HP 35688 selective level meter. Since the bandwidth of the low pass filter is only 7 kHz, the carrier frequency components can be detected alone by setting the frequency of the receiver to the difference frequency, $\omega_m - \omega_b$. The digital readout of the receiver reports the power of the $\omega_m - \omega_b$ component in dBm.

The signal generator for the transducer is turned on and set to a high enough frequency so that the signal will not be in the skirts of the much larger carrier component. A frequency of 2 MHz was chosen for $f_s$ since it was near the optimum frequency of the transducer. Since the signal is found at $\omega_m - \omega_b - \omega_s$, if $\omega_m$ is set to be within several kHz of $\omega_b + \omega_s$ the signal is easily detected within the 7 kHz bandwidth of the low pass filter:

$$\text{for signal frequency} = f_m - f_b - f_s$$

$$\text{choose } f_m = f_b + f_s + 4 \text{ kHz} \quad ,$$

$$\text{then} \qquad \text{signal frequency} = (f_b + f_s + 4 \text{ kHz}) - f_b - f_s$$

$$= 4 \text{ kHz} \quad .$$

Carefully adjusting $f_m$, the maximum power of the signal can be read off the meter.

With these two simple measurements complete, the amplitude of vibration is found immediately using eq. 4.28,

$$\delta_s = \frac{2\lambda_0}{\pi} \left( \frac{P_{m-b-s}}{P_{m-b}} \right)^{\frac{1}{2}} . \qquad (4.28)$$

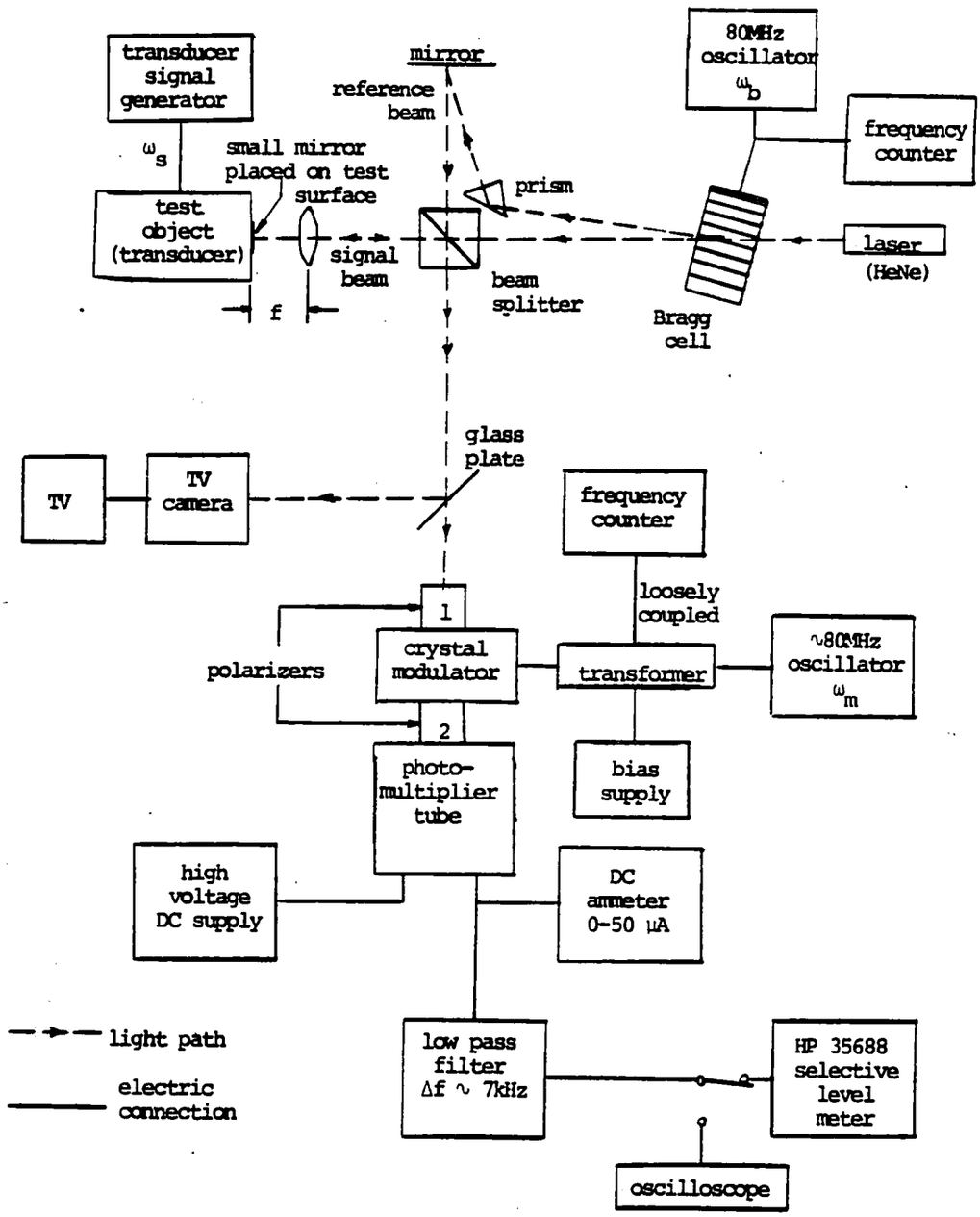


Fig. 6.1 *Optics and block diagram of final system.*

# 7. Results and Conclusions

## 7.1 Results

Initially, the system under test was similar to the one shown in Fig. 4.8, except, instead of a second modulation with the electro-optic modulator and its related electronics, a TIED 96 avalanche photodiode with a preamplifier was placed to detect the light modulated at $f_b$ (80 MHz). A spectrum analyzer was used to view the signals. The carrier component at 80 MHz was successfully detected but, using a calibrated signal generator, its amplitude was found to be only $\sim$400 μV. Considering that the sideband has a much smaller amplitude than the carrier, it was no surprise that the signal was undetectable.

It is of interest at this point to find the theoretical SNR for the system employing the TIED 96. This will aid in the comparison with the system in Fig. 4.8. The TIED 96 was designed to be used optimally at .9 μm and a modulating frequency, $f_m$, of no more than 40 MHz for minimal attenuation. From information given in the manufacturer's specifications sheet and the TI Optoelectronics Data Book (p. 325), it was interpolated that the radiant responsivity, $R_e$, of the detector at $\lambda = 0.633$ μm and $f_m = 80$ MHz was 0.089 mV/nW. The noise equivalent power, NEP, can be found knowing $R_e$;

$$NEP = \frac{V_n}{R_e\sqrt{\tfrac{1}{2}\cdot\pi B_m}} \quad . \tag{7.1}$$

From the spec sheet it is known that $V_n$ = 311 μV and letting $B_m$ = 80 MHz, the NEP is derived to be 0.312 pW/$\sqrt{\text{Hz}}$. The NEP can be related to the quantum efficiency using the following formula[10];

$$q_e = \frac{1.41\sqrt{i_d}}{\text{NEP}} \left( \frac{hf}{\sqrt{e}} \right) \quad . \tag{7.2}$$

Assuming a typical dark current, $i_d$, of $10^{-14}$ A/cm$^2$ over the detector surface area of $5\times10^{-4}$ cm$^2$ and recognizing that $h/\sqrt{e}$ is a constant value of $1.7\times10^{-24}$ and the optical frequency, f, is 474 THz; the quantum efficiency of the TIED 96 at λ = 0.633 μm and $f_m$ = 80 MHz is $8.14\times10^{-6}$.

Since the quantum efficiency has been found, the theoretical SNR (neglecting beam misalignment) can be calculated using eq. 5.15. Recognizing that all the other values are unchanged, the SNR becomes 14.8 dB. Note how close this value is to the SNR of 13.3 dB derived for the system shown in Fig. 4.8, which includes the electro-optic modulator. Recognizing that beam misalignment will affect the SNR in the same way, one immediately concludes that, once this is accounted for the signal will be in the noise. This correlates with the observed result in the laboratory.

When the experimental attempt to use the TIED 96 failed, it was hoped that employing the electro-optic modulator in the system would permit detection of the signal since the demodu-

lation allowed the use of the photomultiplier tube. When this system, as shown in Fig. 4.8, was tested, the carrier component now found at $f_m - f_b$ had approximately the same amplitude as in the previously described system. This correlates well with theory as explained above. Naturally, this meant that the signal was undetectable again.

From these observations, a few important conclusions can be made. Since the theory and laboratory measurements correlate so closely, it can be concluded that a single speckle, within which the light is coherent, does cover the detector surface. The conclusion is valid because this assumption was made in developing the SNR for both systems for which the detector surface areas were different; $S_{d1} = 0.05$ mm$^2$ for the TIED 96 and $S_{d2} = 0.25$ mm$^2$ for the electro-optic modulator. Therefore, since the carrier component amplitudes were so similar for similar theoretical SNR's then a single speckle must have been able to cover the larger surface area of the crystal. Now assured that the speckle size is not the problem, one is led to the conclusion that there is simply not enough light power being reflected off the test surface to be detected with the available equipment.

Since a higher power laser was not available, the measurements had to restricted to specular reflection. This is the system which is physically described at length in section 6 and

is diagrammed in Fig. 6.1. The procedure described previously was followed and both the carrier component and the sidebands were detected. To be assured that the signal detected was in fact the one of interest and not a spurious signal, the signal beam was blocked and the signal disappeared. Also, the voltage to the transducer was reduced to zero and again the signal disappeared. Finally, using frequency counters, it was found that the signal was located exactly at $f_m - f_b - f_s$. The signal moved as $f_m$ was varied and by adjusting $f_m$, it was possible to find the other sideband as well, which was tested in the same way.

Once assured that this was in fact the information carrying signal, the following measurements were made:

$$P_{m-b-s} \text{ (power @ } f = f_m - f_b - f_s) = -34.4 \text{ dBm} = 0.363 \ \mu W$$

and $$P_{m-b} \text{ (power @ } f = f_m - f_b) = 12.0 \text{ dBm} = 15.8 \text{ mW}.$$

Using eq. 4.28, the amplitude of the surface vibration was found to be $\delta_s = 1.93$ nm which is 0.3% of the laser wavelength. This measurement was made with the transducer frequency at 2.1 MHz with an amplitude of 5 V. Keeping the frequency constant, the transducer voltage was decreased which should result in a corresponding decrease of the amplitude of vibration. The results of this test are shown in Fig. 7.1, which shows an approximately linear decrease in signal voltage with decreasing transducer voltage. The dotted line represents the expected values since

the signal voltage, which is proportional to $\delta_s$, should go to zero when the transducer voltage is zero. The actual plot reflects the noise limit since as the signal level approaches the noise level it becomes impossible to detect.

The noise level was measured by turning off the ultrasonic transducer and was found to be -41.3 dBm. The signal - to - noise ratio is experimentally found to be 6.9 dB. Using eq. 5.6 and the values given in Table 5.2, the theoretical SNR can now be recalculated for $\delta_s = 0.003\lambda_0$. Neglecting beam misalignment, the SNR is 11.56 dB. When beam misalignment is considered, a graph similar to Fig. 5.1 may be drawn to reflect the measured value of $\delta_s$. This is shown in Fig. 7.2. Thus assuming the measured value of $\delta_s$ is correct the angle of misalignment is 0.038° which is not a dissapointing value considering the relatively crude and time-consuming method which is used to align the beams.

Confidence in the validity of the $\delta_s$ measurement is high due to the excellent correlation between theory and the results already presented. Nevertheless, an independent verification would be welcome. Unfortunately, the necessary information on the transducer could not be obtained from the manufacturer, ruling out the simplest means of verification. A qualitative test can be made using a simple Michelson interferometer. An interferometer was obtained and one of the mirrors was replaced with the transducer.

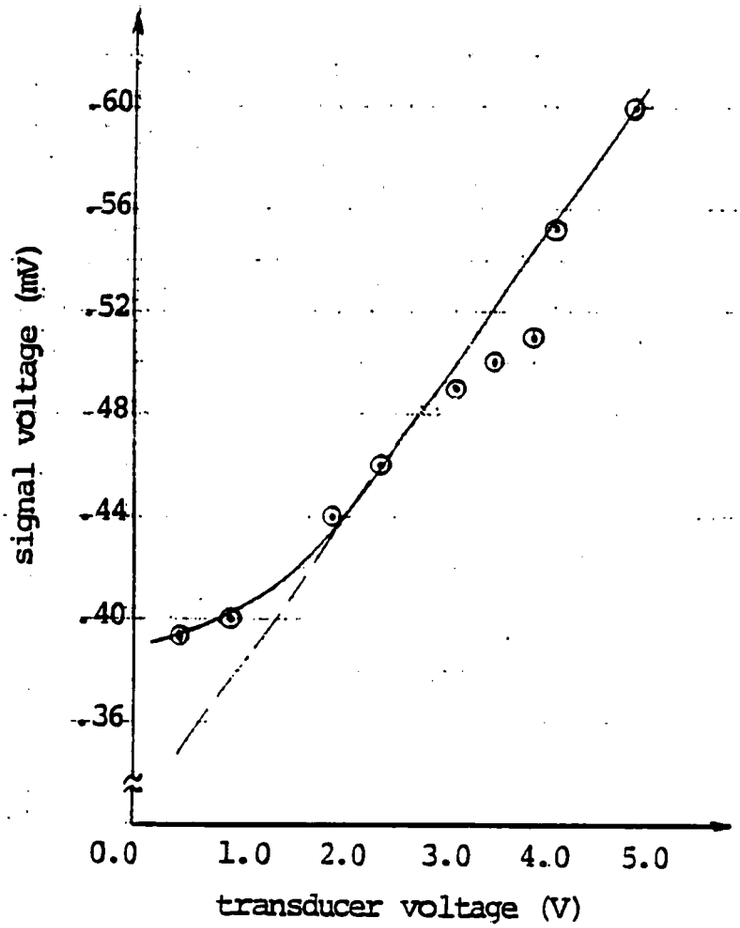


Fig. 7.1 *Signal voltage vs. Transducer voltage : experimental data taken for optical system shown in Fig. 6.1.*

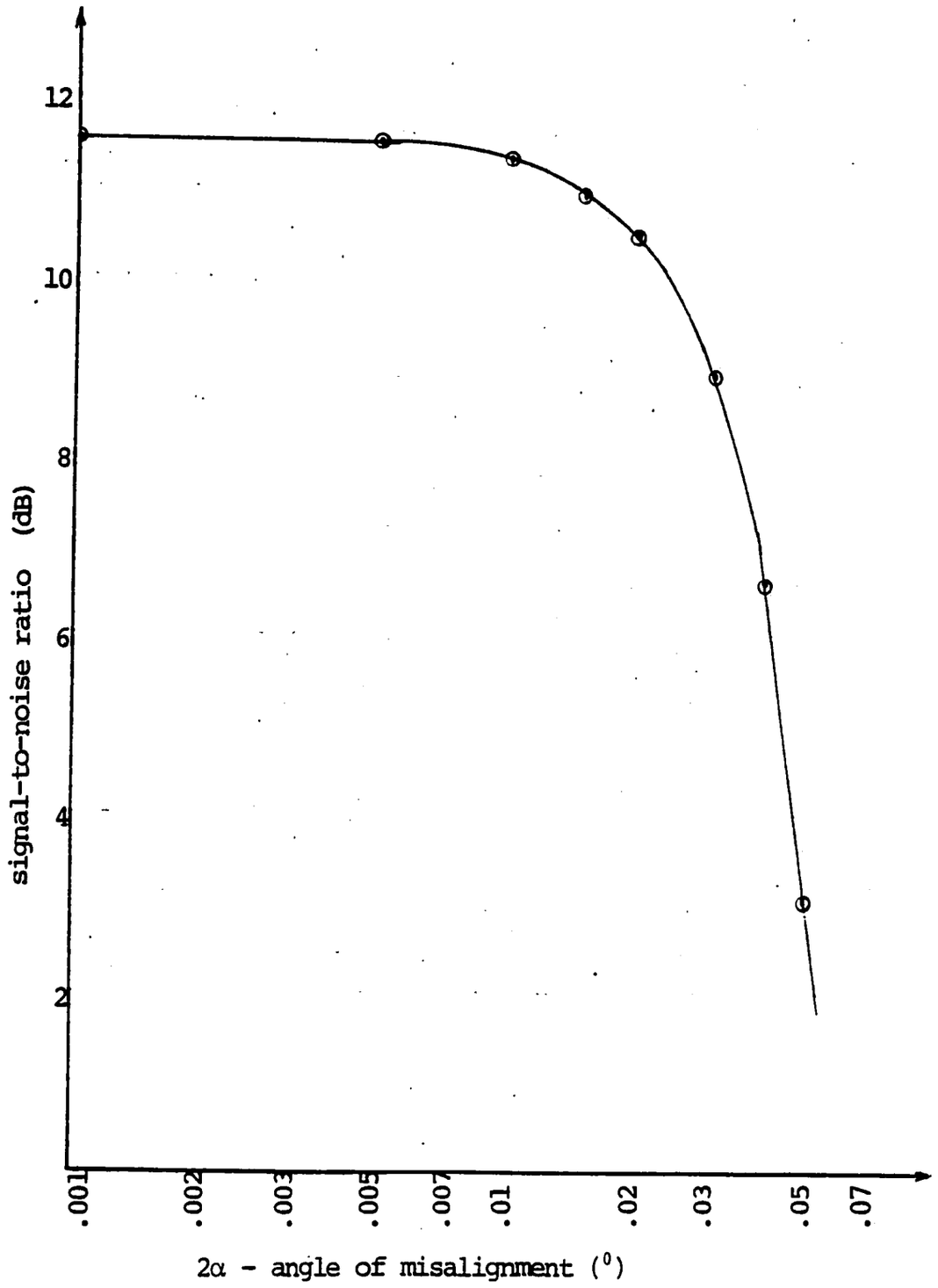


Fig. 7.2 *Theoretical SNR vs. Angle of misalignment for surface vibration* $\delta_s = 0.003\lambda_0$.

The optical set-up of the Michelson interferometer with one of the arms containing the transducer was arranged so that the interference pattern could be viewed on the TV screen. The pathlengths were adjusted so that a clear interference pattern was observed. When adjusted this way, the interference pattern produced by the Michelson interferometer is a series of parallel light and dark fringes where the distance between dark fringes is $\lambda$. When one of the arms of the interferometer is moved $\lambda/2$, the fringe pattern becomes fuzzy and then clear again and the dark fringes interchange with the bright fringes. This is seen clearly from the expression for the intensity of the fringe pattern:

$$I = A^2[1 + \cos(kx\sin\theta + \Delta\psi)] \qquad (7.3)$$

where $\theta$ is the angle that the two wavefronts are inclined to one another at a given point on the screen, $\Delta\psi = k(L_t - L_m)$ is the phase difference caused by the difference in the paths travelled by the light to the transducer ($L_t$) and the mirror ($L_m$), and A is the amplitude of both the beams.

Consider, that in the laboratory, $\Delta\psi$ is such that a bright fringe is in the center of the screen where $\theta = 0°$. Assuming that $L_t - L_m$ is zero, then $I = 2A^2$ at the center of the bright fringe. If the result found for $\delta_s$ is correct then when the transducer signal generator is turned on, the maximum pathlength difference is $0.003\lambda$. This produces a value of $2\pi(0.003)$ for $\Delta\psi$. Substituting this value for $\Delta\psi$ in eq. 7.3 and assuming $\theta = 0°$,

the intensity at the center of the bright fringe is reduced to $1.9998A^2$. Similarly, the dark fringes would become slightly less dark. These are minute changes in the intensities of the fringes, therefore one would suspect that if the value for $\delta_s$ is correct than the human eye would not detect any change (such as *fuzziness*) in the interference pattern when the transducer is turned on. When this test was performed in the laboratory, upon serious scrutinization of the interference pattern on the TV screen, no perceptible change was observed between the patterns with the transducer on and off.

Of course, this is a qualitative result and it leads to the conclusion that $\delta_s = 0.003\lambda_0$ is at least in the same order of magnitude expected. Considering the consistency of the other results, it is very possible that the value measured for $\delta_s$ is fairly accurate. This implies that the device was able to measure a surface vibration of approximately 20 Å and less ! From Fig. 7.1, one can estimate that the signal measured at a transducer voltage of 2.5 V is the last measurement unaffected by the noise. This point corresponds to a surface vibration of 14.6 Å. This sensitivity is comparable to sensitivities reported for other optical heterodyne probes.

## 7.2 Final Conclusions

The results presented correlate well with the theory and confirm that the probe is able to measure small surface vibrations, on the order of tens of angstroms. Unfortunately, this result required an optically polished test surface which may be impractical for certain test environments. If a higher power laser was available, it seems likely that similar sensitivity could be achieved without a reflector. Also, if a device could be designed that tested for and aided in beam alignment, this would certainly help in improving the SNR.

The results also imply that excellent sensitivity could be achieved without the envelope heterodyning if a photodiode was available which could detect signals at a modulating frequency near that of the Bragg cell. But the detection electronics for this system would be much more complex to obtain the same accuracy as obtained for the system discussed in this paper. In appendix A, Fig. 1(b), is an example of the detection electronics needed for such a system. For one, it would require a tunable band pass filter to single out the carrier component and its sidebands, also the very sensitive meter which was used for the envelope heterodyning technique could not have been used since it does not measure high frequencies. Most likely, the signals would have to be electronically demodulated which would further complicate the electronics.

Therefore, it is felt that the technique described in this paper has certain advantages over the other probes, which include simplicity of detection electronics and measurement of signals. Though, the requirement of a higher laser power must also be considered as a disadvantage. It appears that the choice of probes depends heavily upon equipment available and the funds appropriated, since all the probes which are independent of optical phase are practical tools for non-contacting testing of surface vibrations and all have similar sensitivity capabilities.

## REFERENCES


1. De La Rue, R.M., et.al., "Acoustic - Surface - Wave Amplitude and phase measurements using laser probes", Proc. IEE. Vol. 119, No.2, February 1972, p. 117 - 126.

2. Sizgoric, S., et.al., "An Optical Homodyne Technique for Measurement of Amplitude and Phase of Subangstrom Ultrasonic Vibrations", Proc. of the IEEE. July 1969, p. 1313-14.

3. Whitman, R.L. and Korpel, A., "Probing of Acoustic Surface Perturbations by Coherent Light", Applied Optics. Vol. 8, No. 8, August 1969, p. 1567-76.

4. O'Shea, D., Callen, W.R., and Rhodes, W., Introduction to Lasers and their Applications. Addison-Wesley Publishing Co., Mass., 1978.

5. Pohl, R.W., Optik und Atomphysik, p. 65-66, (translated to English by German student).

6. Ishii, K.T., Maser and Laser Engineering. Robert E. Krieger Publishing Co., New York, 1980.

7. Regazzi, J.R.,"Design Study of a LIDAR System for Close Range Distance Measurement", Thesis for M.S.E.E. at Lehigh Univ., 1979. Contained in A Study of CW - LIDAR or Laser Distance Gage.

8. O'Hara, R.T., "Light Modulators at 4 GHz for Continuous Wave Short Range LIDAR", Thesis for M.S.E.E. at Lehigh Univ., 1979. Contained in A Study of CW - LIDAR or Laser Distance Gage.

9. Eberhardt, N., "Summary, Theory, Conclusions", A Study of CW - LIDAR or Laser Distance Gage, Lehigh Univ., 1980.

10. Ross, Monte, Laser Receivers, John Wiley & Sons, Inc., New York, 1967.

11. Durst, F., Melling, A., and Whitelaw, J.H., Principles and Practices of Laser Doppler Anemonetry, Academic Press, London, 1981.

12. Shwartz, M., Infromation, Transmission, Modulation, and Noise, McGraw-Hill Book Co., New York, 1980.

# APPENDIX A - EXAMPLES OF VARIOUS PROBE TYPES

- FIG. 1 PROBE TYPE 5
- FIG. 2 PROBE TYPE 1
- FIG. 3 PROBE TYPE 5
- FIG. 4 PROBE TYPE 7

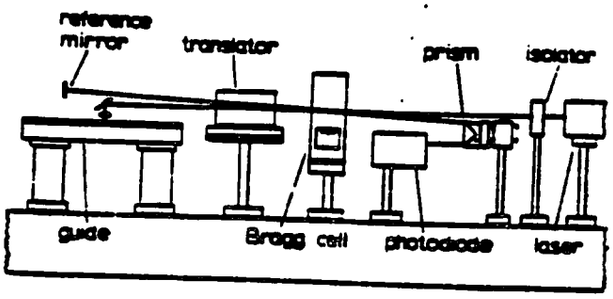


(a)

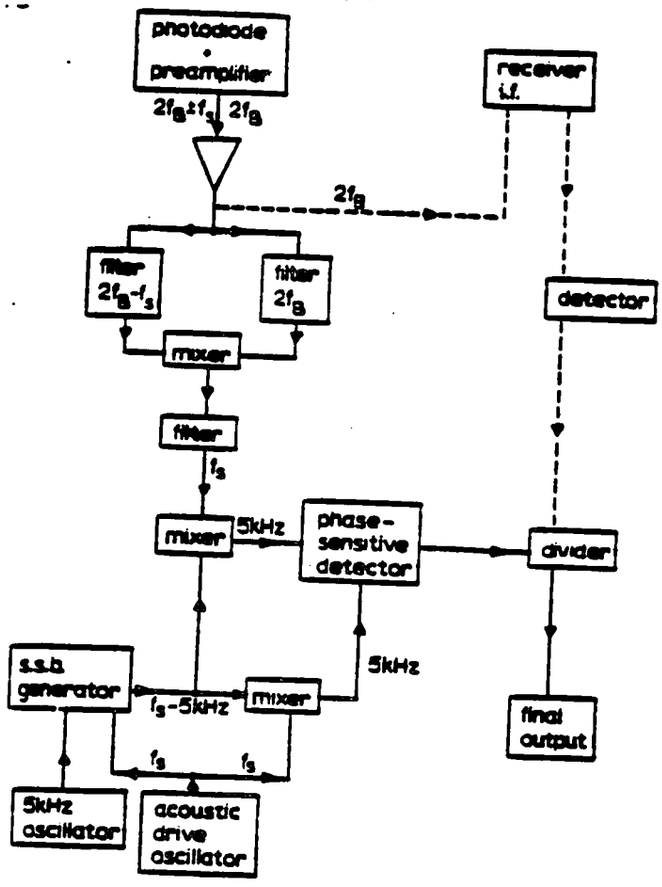


(b)

Fig. 1 Optical Heterodyne System by De La Rue et.al., probe type 5. (a) experimental optical set up. (b) complete detection electronics block diagram.[1]

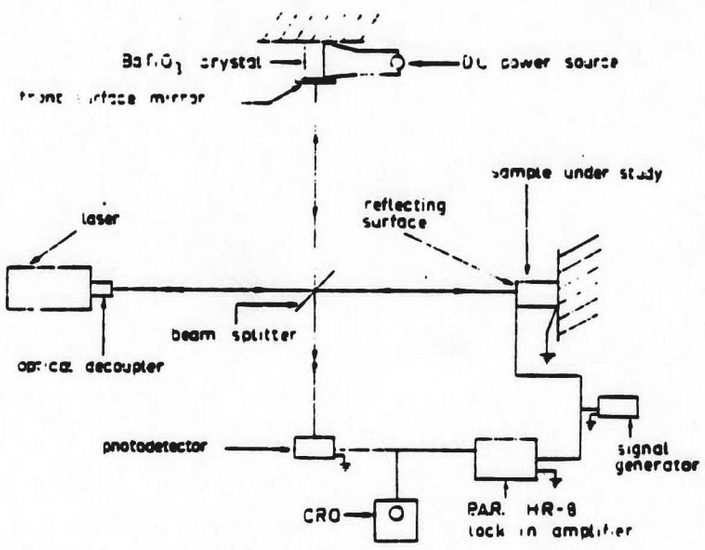


Fig. 2 Optical Homodyne System by Sizgoric et. al., Probe type 1.[2]

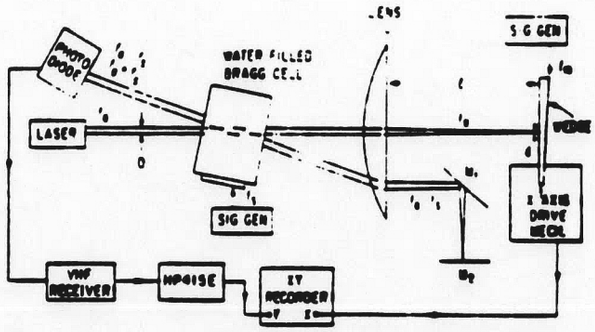


Fig. 3 Optical Heterodyne System by Whitman et.al., Probe type 5.[3]

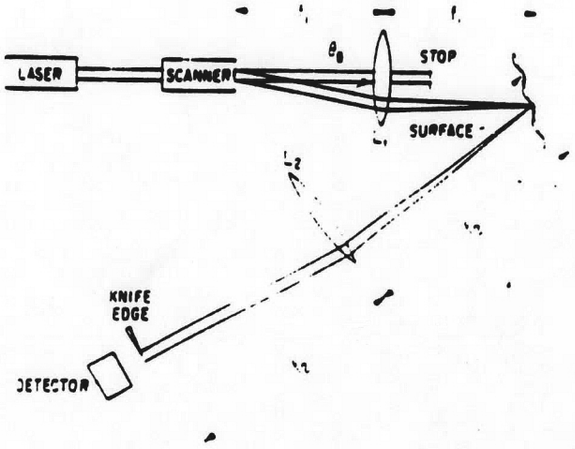


(a)

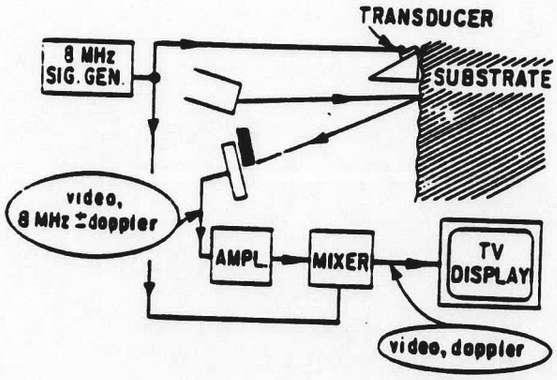


(b)

Fig. 4 Optical Heterodyne System by Adler et. al., Probe type 7. (a) experimental optical set up. (b) block diagram of system omitting optics.[3]

# APPENDIX B - DERIVATION OF FREQUENCY COMPONENTS FOR MODULATION AND DEMODULATION

The signal beam, S, is at the laser frequency, $f_0$, and is modulated by the vibration of the test object at a frequency, $f_s$. The reference beam is at a frequency $f_0 + f_b$, where $f_b$ is the modulating frequency of the Bragg cell.

Therefore, the signal and reference beams at a point directly before the second modulator can be written in the form:

$$S_D = \alpha_S S \exp i\left[k\{L_S + \delta_S \sin(\omega_S t + \theta_S)\} - \omega_0 t\right]$$

$$R_D = \alpha_R R \exp i\left[k L_R - (\omega_0 + \omega_B)t\right] .$$

The light intensity at this point can be described by the following:

$$N_D \propto (S_D + R_D)(S_D^* + R_D^*) = S_D S_D^* + R_D R_D^* + S_D R_D^* + S_D^* R_D .$$

Let $S_D = a + jb$ AND $R_D = c + jd$

where

$$a = \alpha_S S \cos(k\{L_S + \delta_S \sin(\omega_S t + \theta_S)\} - \omega_0 t) = \alpha_S S \cos\alpha$$

$$b = \alpha_S S \sin(k\{L_S + \delta_S \sin(\omega_S t + \theta_S)\} - \omega_0 t) = \alpha_S S \sin\alpha$$

$$c = \alpha_R R \cos(kL_R - (\omega_0 + \omega_B)t) = \alpha_R R \cos\beta$$

$$d = \alpha_R R \sin(kL_R - (\omega_0 + \omega_B)t) = \alpha_R R \sin\beta .$$

Note that:

$$S_D S_D^* = (a+jb)(a-jb) = a^2 + b^2$$

$$R_D R_D^* = c^2 + d^2$$

$$S_D R_D^* = (a+jb)(c-jd) = (ac+bd) + j(bc-ad)$$

$$S_D^* R_D = (a-jb)(c+jd) = (ac+bd) - j(bc-ad) .$$

Then

$$N_d \propto S_0 S_0^* + R_0 R_0^* + S_0 R_0^* + S_0^* R_0 = a^2 + b^2 + c^2 + d^2 + 2(ac+bd)$$

Using the trigonometric identity $\cos^2\theta + \sin^2\theta = 1$, it is easily seen that $a^2+b^2 = \alpha_s^2 S^2$ and $c^2+d^2 = \alpha_R^2 R^2$.

Now must find ac + bd:

$$ac+bd = \alpha_s\alpha_R SR(\cos\alpha\cos\beta + \sin\alpha\sin\beta)$$

$$= \alpha_s\alpha_R SR(\cos(\alpha-\beta)) \qquad \text{(TRIG. IDENTITY)}$$

Replacing in for $\alpha$ and $\beta$:

$$ac+bd = \alpha_s\alpha_R SR\cos\{k[L_s+\delta_s\sin(\omega_s t+\theta_s)] - \omega_0 t - (kL_R - (\omega_0+\omega_B)t)\}$$

$$= \alpha_s\alpha_R SR\cos(k(L_s-L_R) + k\delta_s\sin(\omega_s t+\theta_s) + \omega_B t).$$

Note that $L_s - L_r$ is simply the pathlength difference with no vibration and can be represented by a phase constant:

$$\phi = k(L_s - L_R).$$

Now, the light intensity can be written in the form:

$$N_d \propto \alpha_s^2 S^2 + \alpha_R^2 R^2 + 2\alpha_s\alpha_R SR\cos(\omega_B t + \phi + k\delta_s\sin(\omega_s t+\theta_s)).$$

First, concentrate on the last term:

$$\cos(\omega_B t + \phi + k\delta_s\sin(\omega_s t+\theta_s))$$

$$= \cos\phi\cos(\omega_B t + k\delta_s\sin(\omega_s t+\theta_s)) - \sin\phi\sin(\omega_B t + k\delta_s\sin(\omega_s t+\theta_s))$$

$$= \cos\phi[\cos\omega_B t\cos(k\delta_s\sin(\omega_s t+\theta_s)) - \sin\omega_B t\sin(k\delta_s\sin(\omega_s t+\theta_s))]$$

$$-\sin\phi[\sin\omega_B t\cos(k\delta_s\sin(\omega_s t+\theta_s)) + \cos\omega_B t\sin(k\delta_s\sin(\omega_s t+\theta_s))]$$

The fourier series for $\cos(k\delta_s\sin(\omega_s t+\theta_s))$ and $\sin(k\delta_s\sin(\omega_s t+\theta_s))$ are given by the following:

$$\cos(k\delta_s\sin(\omega_s t+\theta_s)) = J_0(k\delta_s) + 2J_2(k\delta_s)\cos(2(\omega_s t+\theta_s)) + \cdots$$

$$\sin(k\delta_s\sin(\omega_s t+\theta_s)) = 2J_1(k\delta_s)\sin(\omega_s t+\theta_s) + 2J_3(k\delta_s)\sin(3(\omega_s t+\theta_s)) + \cdots$$

Using the above equations and trigonometric product relations,

then:

$$\cos\omega_B t \cos(k\delta_s \sin(\omega_s t+\theta_s)) - \sin\omega_B t \sin(k\delta_s \sin(\omega_s t+\theta_s))$$

$$= J_0(k\delta_s)\cos\omega_B t - J_1(k\delta_s)\left[\cos((\omega_B-\omega_s)t-\theta_s) - \cos((\omega_B+\omega_s)t+\theta_s)\right] + \cdots$$

and

$$\sin\omega_B t \cos(k\delta_s \sin(\omega_s t+\theta_s)) + \cos\omega_B t \sin(k\delta_s \sin(\omega_s t+\theta_s))$$

$$= J_0(k\delta_s)\sin\omega_B t + J_1(k\delta_s)\left[\sin((\omega_B+\omega_s)t+\theta_s) + \sin((\omega_B-\omega_s)t-\theta_s)\right] + \cdots .$$

Thus $\cos(\omega_B t+\phi+k\delta_s \sin(\omega_s t+\theta_s))$

$$= J_0(k\delta_s)\left[\cos\omega_B t\cos\phi + \sin\omega_B t\sin\phi\right]$$
$$+ J_1(k\delta_s)\left[\sin\phi\left\{\sin((\omega_B+\omega_s)t+\theta_s) + \sin((\omega_B-\omega_s)t-\theta_s)\right\}\right.$$
$$\left. -\cos\phi\left\{\cos((\omega_B-\omega_s)t-\theta_s) - \cos((\omega_B+\omega_s)t+\theta_s)\right\}\right] .$$

The final result for the light intensity can now be written as:

$$N_d \propto \alpha_s^2 S^2 + \alpha_R^2 R^2 + 2\alpha_s\alpha_R SR\left[J_0(k\delta_s)\left[\sin\phi\sin\omega_B t + \cos\phi\cos\omega_B t\right]\right.$$
$$+ J_1(k\delta_s)\left[\sin\phi\left\{\sin((\omega_B+\omega_s)t+\theta_s) + \sin((\omega_B-\omega_s)t-\theta_s)\right\}\right.$$
$$\left.\left. -\cos\phi\left\{\cos((\omega_B-\omega_s)t-\theta_s) - \cos((\omega_B+\omega_s)t+\theta_s)\right\}\right]\right] .$$

For determination of the frequency response, determine the power of the light at the different frequencies:

DC component: $\alpha_s^2 S^2 + \alpha_R^2 R^2$

$\omega_B$ component: $\left[2\alpha_s\alpha_R SR\, J_0(k\delta_s)\sin\phi\right]^2 + \left[2\alpha_s\alpha_R SR\, J_0(k\delta_s)\cos\phi\right]^2$
$= 4\alpha_s^2\alpha_R^2 S^2 R^2 J_0^2(k\delta_s)$

$\omega_B+\omega_s$ component: $\left[2\alpha_s\alpha_R SR J_1(k\delta_s)\sin\phi\right]^2 + \left[2\alpha_s\alpha_R SR J_1(k\delta_s)\cos\phi\right]^2$
$= 4\alpha_s^2\alpha_R^2 S^2 R^2 J_1^2(k\delta_s)$

$\omega_B-\omega_s$ component: $4\alpha_s^2\alpha_R^2 S^2 R^2 J_1^2(k\delta_s)$

In the lab, the demodulation is accomplished with a light modulator using the linear optoelectric effect (Poeckel's effect):

$$S = \sin^2(\Gamma/2) \qquad \text{where} \qquad \frac{\Gamma}{2} = \frac{m\pi}{2}\sin\omega_m t + B\pi$$

This is shown in the figure below:

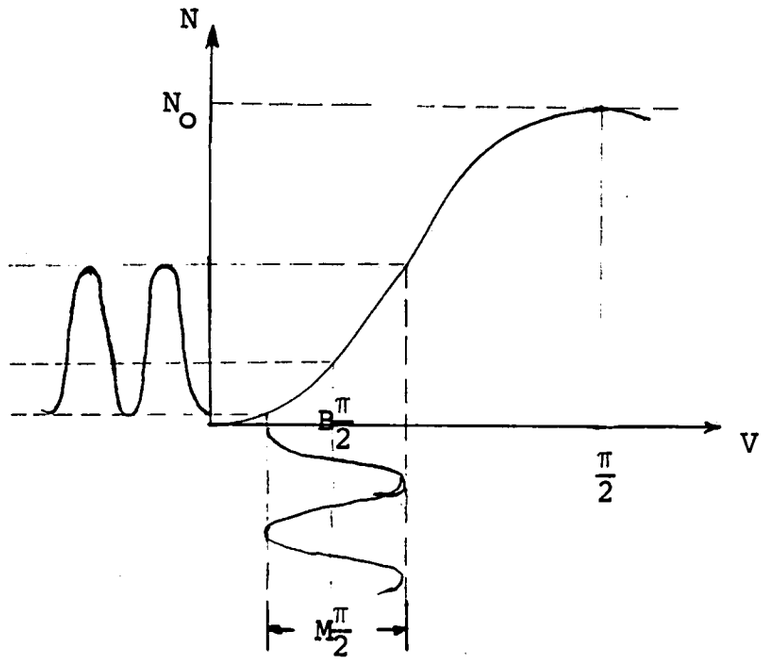


Now, must find the frequency response if the light is modulated again with the electrooptic modulator with the above modulating characteristic. The light intensity resulting from this second modulation is given by:

$$N_{dm} \propto (\alpha_s^2 S^2 + \alpha_R^2 R^2)\sin^2\left(\frac{m\pi}{2}\sin\omega_m t + B\pi\right) +$$
$$2\alpha_s\alpha_R SR \sin^2\left(\frac{m\pi}{2}\sin\omega_m t + B\pi\right)\Big[J_0(K\delta_s)(\sin\phi\sin\omega_B t + \cos\phi\cos\omega_B t)$$
$$+ J_0(K\delta_s)\Big[\sin\phi\{\sin((\omega_B+\omega_s)t+\theta_s) + \sin((\omega_B-\omega_s)t-\theta_s)\}$$
$$-\cos\phi\{\cos((\omega_B-\omega_s)t-\theta_s) - \cos((\omega_B+\omega_s)t+\theta_s)\}\Big] + \cdots\Big]$$

Using trigonometric identities:

$$\sin^2\left(\tfrac{m\pi}{2}\sin\omega_m t+B\pi\right)=\tfrac{1}{2}-\tfrac{1}{2}\cos\left(2\left(\tfrac{m\pi}{2}\sin\omega_m t+B\pi\right)\right)$$

$$=\tfrac{1}{2}-\tfrac{1}{2}\left(\cos B\pi\cos\left(\tfrac{m\pi}{2}\sin\omega_m t\right)-\sin B\pi\sin\left(\tfrac{m\pi}{2}\sin\omega_m t\right)\right)$$

$$=\tfrac{1}{2}\left[1-\cos B\pi\cos\left(\tfrac{m\pi}{2}\sin\omega_m t\right)+\sin B\pi\sin\left(\tfrac{m\pi}{2}\sin\omega_m t\right)\right]$$

$$=\tfrac{1}{2}\Big[1-\left[J_0\left(\tfrac{m\pi}{2}\right)+2J_2\left(\tfrac{m\pi}{2}\right)\cos 2\omega_m t+\cdots\right]\cos B\pi$$

$$+\left[2J_1\left(\tfrac{m\pi}{2}\right)\sin\omega_m t+2J_3\left(\tfrac{m\pi}{2}\right)\sin 3\omega_m t+\cdots\right]\sin B\pi\Big].$$

Using only the $J_0\left(\frac{m\pi}{2}\right)$ and $J_1\left(\frac{m\pi}{2}\right)$ terms and replacing into the equation for $N_{dm}$, yields:

$$N_{dm}\propto\tfrac{1}{2}\left(\alpha_S^2S^2+\alpha_R^2R^2\right)-\tfrac{1}{2}\left(\alpha_S^2S^2+\alpha_R^2R^2\right)\cos B\pi\,J_0\left(\tfrac{m\pi}{2}\right)+ \qquad \text{(LINE 1)}$$

$$\left(\alpha_S^2S^2+\alpha_R^2R^2\right)J_1\left(\tfrac{m\pi}{2}\right)\sin B\pi\sin\omega_m t$$

$$+\alpha_S\alpha_R SRJ_0(K\delta_S)\left(\sin\phi\sin\omega_B t+\cos\phi\cos\omega_B t\right) \qquad \text{(LINE 2)}$$

$$-\alpha_S\alpha_R SRJ_0\left(\tfrac{m\pi}{2}\right)\cos B\pi\,J_0(K\delta_S)\left(\sin\phi\sin\omega_B t+\cos\phi\cos\omega_B t\right) \qquad \text{(LINE 3)}$$

$$+2\alpha_S\alpha_R SRJ_1\left(\tfrac{m\pi}{2}\right)\sin B\pi\,J_0(K\delta_S)\sin\omega_m t\left(\sin\phi\sin\omega_B t+\cos\phi\cos\omega_B t\right) \qquad \text{(LINE 4)}$$

$$+\alpha_S\alpha_R SRJ_1(K\delta_S)\Big[\sin\phi\left\{\sin\left((\omega_B+\omega_S)t+\theta_S\right)+\sin\left((\omega_B-\omega_S)t-\theta_S\right)\right\} \qquad \text{(LINE 5)}$$

$$-\cos\phi\left\{\cos\left((\omega_B-\omega_S)t-\theta_S\right)-\cos\left((\omega_B+\omega_S)t+\theta_S\right)\right\}\Big]$$

$$-\alpha_S\alpha_R SRJ_0\left(\tfrac{m\pi}{2}\right)\cos B\pi\,J_1(K\delta_S)\Big[\sin\phi\left\{\sin\left((\omega_B+\omega_S)t+\theta_S\right)+\sin\left((\omega_B-\omega_S)t-\theta_S\right)\right\} \qquad \text{(LINE 6)}$$

$$-\cos\phi\left\{\cos\left((\omega_B-\omega_S)t-\theta_S\right)-\cos\left((\omega_B+\omega_S)t+\theta_S\right)\right\}\Big]$$

$$+2\alpha_S\alpha_R SRJ_1\left(\tfrac{m\pi}{2}\right)\sin B\pi\,J_1(K\delta_S)\sin\omega_m t\Big[\sin\phi\left\{\sin\left((\omega_B+\omega_S)t+\theta_S\right)\right. \qquad \text{(LINE 7)}$$

$$\left.+\sin\left((\omega_B+\omega_S)t+\theta_S\right)\right\}$$

$$-\cos\phi\left\{\cos\left((\omega_B-\omega_S)t-\theta_S\right)-\cos\left((\omega_B+\omega_S)t+\theta_S\right)\right\}\Big].$$

No further trigonometric reductions are necessary for lines

1, 2, 3, 5, and 6.

line 4:

$$2\alpha_S\alpha_R SRJ_1\left(\tfrac{m\pi}{2}\right)\sin B\pi J_0(k\delta_S)\left(\sin\phi\sin\omega_m t\sin\omega_B t+\cos\phi\sin\omega_m t\cos\omega_B t\right)$$

$$=2\alpha_S\alpha_R SRJ_1\left(\tfrac{m\pi}{2}\right)\sin B\pi J_0(k\delta_S)\Big[\tfrac{1}{2}\sin\phi\left(\cos(\omega_m-\omega_B)t-\cos(\omega_m+\omega_B)t\right)$$
$$+\tfrac{1}{2}\cos\phi\left(\sin(\omega_m+\omega_B)t+\sin(\omega_m-\omega_B)t\right)\Big]$$

$$=\alpha_S\alpha_R SRJ_1\left(\tfrac{m\pi}{2}\right)\sin B\pi J_0(k\delta_S)\Big[\sin\phi\left(\cos(\omega_m-\omega_B)t-\cos(\omega_m+\omega_B)t\right)$$
$$+\cos\phi\left(\sin(\omega_m+\omega_B)t+\sin(\omega_m-\omega_B)t\right)\Big]\ .$$

line 7:

$$2\alpha_S\alpha_R SRJ_1\left(\tfrac{m\pi}{2}\right)\sin B\pi J_1(k\delta_S)\Big[\sin\phi\left[\sin\omega_m t\left(\sin((\omega_B+\omega_S)t+\theta_S)+\sin((\omega_B-\omega_S)t-\theta_S)\right)\right]$$
$$-\cos\phi\left[\sin\omega_m t\cos((\omega_B-\omega_S)t-\theta_S)-\sin\omega_m t\cos((\omega_B+\omega_S)t+\theta_S)\right]\Big]$$

$$=2\alpha_S\alpha_R SRJ_1\left(\tfrac{m\pi}{2}\right)\sin B\pi J_1(k\delta_S)\Big[\tfrac{\sin\phi}{2}\left[\cos((\omega_m-\omega_B-\omega_S)t-\theta_S)-\cos((\omega_m+\omega_B+\omega_S)t+\theta_S)\right.$$
$$\left.+\cos((\omega_m-\omega_B+\omega_S)t+\theta_S)-\cos((\omega_m+\omega_B-\omega_S)t-\theta_S)\right]$$
$$-\tfrac{\cos\phi}{2}\left[\sin((\omega_m+\omega_B-\omega_S)t-\theta_S)+\sin((\omega_m-\omega_B+\omega_S)t+\theta_S)\right.$$
$$\left.-\sin((\omega_m+\omega_B+\omega_S)t+\theta_S)-\sin((\omega_m-\omega_B-\omega_S)t-\theta_S)\right]\Big]\ .$$

The expression for the light intensity after modulation is given by:

$$N_{dm}\propto\tfrac{X}{2}-\tfrac{X}{2}\cos B\pi J_0\left(\tfrac{m\pi}{2}\right)+X\sin B\pi J_1\left(\tfrac{m\pi}{2}\right)\sin\omega_m t$$
$$+Y(\sin\phi\sin\omega_B t+\cos\phi\cos\omega_B t)\left(1-\cos B\pi J_0\left(\tfrac{m\pi}{2}\right)\right)$$
$$+2Y\sin B\pi J_1\left(\tfrac{m\pi}{2}\right)\Big[\sin\phi\left\{\cos((\omega_m-\omega_B)t)-\cos((\omega_m+\omega_B)t)\right\}$$
$$+\cos\phi\left\{\sin((\omega_m+\omega_B)t+\sin(\omega_m-\omega_B)t)\right\}\Big]$$
$$+Z\Big[\sin\phi\left[\sin((\omega_B+\omega_S)t+\theta_S)+\sin((\omega_B-\omega_S)t-\theta_S)\right]$$
$$-\cos\phi\left[\cos((\omega_B-\omega_S)t-\theta_S)-\cos((\omega_B+\omega_S)t+\theta_S)\right]\Big]\left(1-\cos B\pi J_0\left(\tfrac{m\pi}{2}\right)\right)$$
$$+2\sin B\pi J_1\left(\tfrac{m\pi}{2}\right)\sin\phi\Big[\cos((\omega_m-\omega_B-\omega_S)t-\theta_S)-\cos((\omega_m+\omega_B+\omega_S)t-\theta_S)$$
$$+\cos((\omega_m-\omega_B+\omega_S)t+\theta_S)-\cos((\omega_m+\omega_B+\omega_S)t-\theta_S)\Big]$$
$$+2\sin B\pi J_1\left(\tfrac{m\pi}{2}\right)\cos\phi\Big[\sin((\omega_m+\omega_B-\omega_S)t-\theta_S)+\sin((\omega_m-\omega_B+\omega_S)t+\theta_S)$$
$$-\sin((\omega_m+\omega_B+\omega_S)t+\theta_S)-\sin((\omega_m+\omega_B-\omega_S)t-\theta_S)\Big]$$

where $X = (\alpha_s^2 S^2 + \alpha_R^2 R^2)$

$Y = \alpha_s \alpha_R SR J_0(k\delta_s)$

and $Z = \alpha_s \alpha_R SR J_1(k\delta_s)$ .

For $\omega_B \neq \omega_m$, the power detected at the different frequencies will be:

DC component: $\frac{1}{2}(\alpha_s^2 S^2 + \alpha_R^2 R^2)(1 - \cos B\pi J_0(\frac{m\pi}{2}))$

$\omega_B$ component: $[\alpha_s \alpha_R SR J_0(k\delta_s)(1 - \cos B\pi)]^2$

$\omega_m$ component: $[(\alpha_s^2 S^2 + \alpha_R^2 R^2) J_1(\frac{m\pi}{2}) \sin B\pi]^2$

$\omega_m + \omega_B$ and $\omega_m - \omega_B$ component: $[2\alpha_s \alpha_R SR J_1(\frac{m\pi}{2}) \sin B\pi J_0(k\delta_s)]^2$

$\omega_B + \omega_s$ and $\omega_m - \omega_B$ component: $[\alpha_s \alpha_R SR J_1(k\delta_s)(1 - \cos B\pi)]^2$

$\omega_m + \omega_B + \omega_s$ and $\omega_m - \omega_B - \omega_s$ and $\omega_m - \omega_B + \omega_s$ and $\omega_m + \omega_B - \omega_s$ component: $[\alpha_s \alpha_R SR J_1(\frac{m\pi}{2}) \sin B\pi J_1(k\delta_s)]^2$

# APPENDIX C - SNR CALCULATIONS - OPTICAL HOMODYNE SYSTEM

Using the general equations given in the text of the report (eq. 2.1), the signal and reference beams at the detector can be found. For the homodyne technique p = q = 0 and = 0, thus $S_d$ and $R_d$ are given by:

$$S_o = \alpha_s S \exp i\left[k\{L_s + \delta_s \cos(\omega_s t + \theta_s)\} - \omega_o t\right]$$

and $$R_o = \alpha_R R \exp i\left[kL_R - \omega_o t\right] .$$

The light intensity is

$$N_d \propto (S_o + R_o)(S_o^* + R_o^*) = S_o S_o^* + R_o R_o^* + S_o^* R_o + S_o R_o^* .$$

Let $S_d = a + jb$ and $R_d = c + jd$, where a, b, c, and d are:

$$a = \alpha_s S \cos(k\{L_s + \delta_s \sin(\omega_s t + \theta_s)\} - \omega_o t) = \alpha_s S \cos\alpha$$

$$b = \alpha_s S \sin(k\{L_s + \delta_s \sin(\omega_s t + \theta_s)\} - \omega_o t) = \alpha_s S \sin\alpha$$

$$c = \alpha_R R \cos(kL_R - \omega_o t) = \alpha_R R \cos\beta$$

$$d = \alpha_R R \sin(kL_R - \omega_o t) = \alpha_R R \sin\beta .$$

Note that

$$S_d S_d^* = a^2 + b^2$$

$$R_d R_d^* = c^2 + b^2$$

$$S_d R_d^* = (ac + bd) + j(bc - ad)$$

$$S_d^* R_d = (ac + bd) - j(bc - ad)$$

and then

$$N_d \propto (a^2 + b^2) + (c^2 + d^2) + 2(ac + bd) .$$

Using various trigonometric identities:

$$a^2 + b^2 = (\alpha_s S)^2 \qquad c^2 + d^2 = (\alpha_R R)^2$$

and $$ac + bd = \alpha_s \alpha_R SR \cos(k(L_s - L_R) + k\delta_s \sin(\omega_s t + \theta_s)) .$$

Note that $k(L_s - L_r)$ is simply the pathlength difference with no vibration and can be represented by a phase constant

$$\phi = k(L_s - L_R) .$$

Now, $N_d$ can be written as

$$N_d \propto (\alpha_s S)^2 + (\alpha_R R)^2 + 2\alpha_s \alpha_R SR \cos(\phi + k\delta_s \sin(\omega_s t + \theta_s)) .$$

Using trigonometric identities and the fourier series given in eqs. 4.18 in the text of the report, the final form is written as:

$$N_d \propto (\alpha_s S)^2 + (\alpha_R R)^2 + 2\alpha_s \alpha_R SR[\cos\phi J_0(k\delta_s) - \sin\phi 2J_1(k\delta_s)\sin(\omega_s t + \theta_s) + \cos\phi 2J_2(k\delta_s)\cos(2\omega_s t + 2\theta_s)] .$$

The power in the components is proportional to amplitude squared:

DC component: $(\alpha_s S)^2 + (\alpha_R R^2) + 2\alpha_s \alpha_R SR \cos\phi J_0(k\delta_s)$

$\omega_s$ component: $[4\alpha_s \alpha_R SR \sin\phi J_1(k\delta_s)]^2$

$2\omega_s$ component: $[4\alpha_s \alpha_R SR \cos\phi J_2(k\delta_s)]^2$ .

Assuming the configuration shown in Fig. 5.2 in the text, the SNR of the system may be derived. Initially, the attenuations of the signal and reference beams, $\alpha_s$ and $\alpha_R$, must be found. Since there is no significant change in the path followed by the signal beam, the same value used for the heterodyne system can be assumed: $(\alpha_s S)^2 = 0.24\,\mu W$. The path of the reference beam has changed from the initial set-up, therefore its attenuation must be recalculated. The calculations for $(\alpha_R R)^2$ are shown in the table on the following page where the values are obtained from measurements in the laboratoryor estimated from information in Reference 9.

attenuation of reference beam

| | | |
|---|---|---|
| laser output | 2.1 mW | |
| pass through beam splitter | 1.0 mW | 3.78 dB |
| attenuation of beam splitter | .419 mW | 1.20 dB |
| mirror | .318 mW | 7.56 dB |
| attenuation of beam splitter | 55.7 μW | |
| | total attenuation of reference beam | 12.54 dB |

Therefore, $(\alpha_R R)^2 = 55.7\ \mu W$.

The SNR is given by:

$$\frac{I^2_{RMS}}{\bar{i}^2} = \frac{\eta_e}{2h\nu a^2 \Delta f} \frac{N^2_{RMS}}{\bar{N}}$$

where $N^2_{RMS} = 16(\alpha_S S)^2(\alpha_R R)^2 \sin^2\phi\, J_1^2(k\delta_S)$

and $\bar{N} = (\alpha_S S)^2 + (\alpha_R R)^2 + 2(\alpha_S S)(\alpha_R R)\cos\phi\, J_0(k\delta_S)$.

Thus:

$$\frac{I^2_{RMS}}{\bar{i}^2} = \frac{16\eta_e}{h\nu a^2 \Delta f} \frac{(\alpha_S S)^2(\alpha_R R)^2 \sin^2\phi\, J_1^2(k\delta_S)}{[(\alpha_S S)^2 + (\alpha_R R)^2 + 2(\alpha_S S)(\alpha_R R)\cos\phi\, J_0(k\delta_S)]}.$$

Choosing the same values as in the text, then:

| parameter | value |
|---|---|
| $(\alpha_S S)^2$ | 0.24 μW |
| $(\alpha_R R)^2$ | 55.7 μW |
| $\Delta f$ | 7 KHz |
| $\eta_e$ | .05 |
| $h\nu$ | $3.14 \times 10^{-19}$ |
| $\delta_S$ | $.05\lambda_0$ |

First, to determine the maximum SNR, $\sin^2\phi$ must be maximum. This occurs when $\phi = k(L_s - L_r) = \frac{1}{2}n\pi$ $(n = 1,3,\ldots)$. Therefore, for maximum SNR choose $L_s - L_r = \frac{1}{4}\lambda$ . Replacing all these values into the given equation then

$$SNR_{max} = 58.7 \text{ dB} \quad .$$

Note, when $\sin^2\phi = 0$, the signal becomes non-existent !

# APPENDIX D - DATA AND TABLES

- TABLE OF EXPERIMENTAL RESULTS
- TABLE OF SIGNAL - TO - NOISE RATIO

V. VS.

ANGLE OF MISALIGNMENT

## EXPERIMENTAL RESULTS

| transducer amplitude (V) | signal level (dBm) | signal power $P_s$ (nW) | signal voltage $\alpha (P_s)^{\frac{1}{2}}$ (mV) |
|---|---|---|---|
| 5.0 | -34.4 | 363 | .602 |
| 4.2 | -35.15 | 305 | .552 |
| 4.0 | -35.9 | 257 | .507 |
| 3.6 | -36.0 | 251 | .501 |
| 3.2 | -36.2 | 240 | .490 |
| 2.5 | -36.8 | 209 | .457 |
| 2.0 | -37.1 | 195 | .442 |
| 1.0 | -37.95 | 160 | .400 |
| 0.5 | -38.10 | 155 | .394 |

SIGNAL - TO - NOISE RATIO VS. ANGLE OF MISALIGNMENT

| $2\alpha$ ($^0$) | SNR for $\delta_s = .05\lambda_0$ (dB) | SNR for $\delta_s = .003\lambda_0$ (dB) |
|---|---|---|
| .001 | 35.87 | 11.56 |
| .005 | 35.80 | 11.49 |
| .01 | 35.59 | 11.28 |
| .015 | 35.24 | 10.93 |
| .02 | 34.74 | 10.44 |
| .03 | 33.23 | 8.92 |
| .04 | 30.90 | 6.60 |
| .05 | 27.36 | 3.06 |
| .06 | 21.49 | -2.8 |
| .065 | 16.38 | -7.9 |
| .07 | 4.98 | -19.3 |

**LEAH M. AKINS**

**PERSONAL**

| Home Address | Business Address |
|---|---|
| 215 McCartney St.<br>Easton, PA 18042<br>(215) 250-0863<br>Birth Date: 5-17-61 | Lafayette College<br>Easton, PA 18042<br>(215) 250-5420 |

**JOB OBJECTIVE**

Summer engineering position that will allow the practical application of my knowledge.

**EDUCATION**

May 1985 - M.S. Electrical Engineering
Lehigh University, Bethlehem, Pennsylvania
Courses included **Nonlinear Optics, Microwave Devices,** and **Theory of Mathematical Physics.**

Thesis: " **Optical Detection of Surface Vibrations**", results included the detection of vibrations on the order of 5-10% of the laser wavelength (HeNe=633nm).

May 1982 - B.S. Electrical Engineering
Lafayette College, Easton, Pennsylvania
Courses included **Laser Engineering** and **Microwave Engineering.**

**HONORS AND ACTIVITIES**

Dean's List, Lafayette College, 1980-82
Eta Kappa Nu, Electrical Engineering Honor Society
Member of IEEE

**EXPERIENCE**

Sept. 1982 - Present — **Lab Associate in Electrical Engineering,** Lafayette College, Easton, PA. Responsibilities include the supervision and instruction of the Electronics labs. In charge of ordering parts, supervising maintenance of the lab, and coordinating the different lab sections. Also teach Digital and Machines laboratories.

Summer 1982 — **ENGINEER**, Narda Microwave, Hauppauge, N.Y. Worked on a narrow-band microwave filter and related software which analized insertion loss and return loss for varying parameters of the microwave cavity. Also worked on a microstrip "friend or foe" system.

Summer 1981 — **Jr. Engineer**, New York Telephone Co., N.Y., N.Y. Project was development and execution of energy conservation audit for N.Y. Telephone Co. buildings.